

You might find this additional information useful...

This article cites 60 articles, 34 of which you can access free at:

<http://jn.physiology.org/cgi/content/full/78/2/1045#BIBL>

This article has been cited by 28 other HighWire hosted articles, the first 5 are:

The Spatiotemporal Frequency Tuning of LGN Receptive Field Facilitates Neural Discrimination of Natural Stimuli

Z. Tan and H. Yao

J. Neurosci., September 9, 2009; 29 (36): 11409-11416.

[Abstract] [Full Text] [PDF]

Functional Consequences of Neuronal Divergence Within the Retinogeniculate Pathway

C.-I Yeh, C. R. Stoelzel, C. Weng and J.-M. Alonso

J Neurophysiol, April 1, 2009; 101 (4): 2166-2185.

[Abstract] [Full Text] [PDF]

Time Course of Cross-Orientation Suppression in the Early Visual Cortex

R. Kimura and I. Ohzawa

J Neurophysiol, March 1, 2009; 101 (3): 1463-1479.

[Abstract] [Full Text] [PDF]

Dynamics of Spatial Resolution of Single Units in the Lateral Geniculate Nucleus of Cat During Brief Visual Stimulation

O. Ruksenas, A. Bulatov and P. Heggelund

J Neurophysiol, February 1, 2007; 97 (2): 1445-1456.

[Abstract] [Full Text] [PDF]

Dynamic spatial processing originates in early visual pathways.

E. A. Allen and R. D. Freeman

J. Neurosci., November 8, 2006; 26 (45): 11763-11774.

[Abstract] [Full Text] [PDF]

Medline items on this article's topics can be found at <http://highwire.stanford.edu/lists/artbytopic.dtl> on the following topics:

Veterinary Science .. Lateral Geniculate Nucleus

Physiology .. Action Potential

Veterinary Science .. Dogs

Physiology .. Cats

Updated information and services including high-resolution figures, can be found at:

<http://jn.physiology.org/cgi/content/full/78/2/1045>

Additional material and information about *Journal of Neurophysiology* can be found at:

<http://www.the-aps.org/publications/jn>

This information is current as of November 11, 2009 .

Spatiotemporal Receptive Field Organization in the Lateral Geniculate Nucleus of Cats and Kittens

DAQING CAI, GREGORY C. DEANGELIS, AND RALPH D. FREEMAN

Group in Vision Science, School of Optometry, University of California, Berkeley, California 94720-2020

Cai, Daqing, Gregory C. DeAngelis, and Ralph D. Freeman. Spatiotemporal receptive field organization in the lateral geniculate nucleus of cats and kittens. *J. Neurophysiol.* 78: 1045–1061, 1997. We have studied the spatiotemporal receptive-field organization of 144 neurons recorded from the dorsal lateral geniculate nucleus (dLGN) of adult cats and kittens at 4 and 8 wk postnatal. Receptive-field profiles were obtained with the use of a reverse correlation technique, in which we compute the cross-correlation between the action potential train of a neuron and a randomized sequence of long bright and dark bar stimuli that are flashed throughout the receptive field. Spatiotemporal receptive-field profiles of LGN neurons generally exhibit a biphasic temporal response, as well as the classical center-surround spatial organization. For nonlagged cells, the first temporal phase of the response dominates, whereas for lagged neurons, the second temporal phase of the response is typically the largest. This temporal phase difference between lagged and nonlagged cells accounts for their divergent behavior in response to flashed stimuli. Most LGN cells exhibit some degree of space-time inseparability, which means that the receptive field cannot simply be viewed as the product of a spatial waveform and a temporal waveform. In these cases, the response of the surround is typically delayed relative to that of the center, and there is some blending of center and surround during the time course of the response. We demonstrate that a simple extension of the traditional difference-of-Gaussians (DOG) model, in which the surround response is delayed relative to that of the center, accounts nicely for these findings. With regard to development, our analysis shows that spatial and temporal aspects of receptive field structure mature with markedly different time courses. After 4 wk postnatal, there is little change in the spatial organization of LGN receptive fields, with the exception of a weak, but significant, trend for the surround to become smaller and stronger with age. In contrast, there are substantial changes in temporal receptive-field structure after 4 wk postnatal. From 4 to 8 wk postnatal, the shape of the temporal response profile changes, becoming more biphasic, but the latency and duration of the response remain unchanged. From 8 wk postnatal to adulthood, the shape of the temporal profile remains approximately constant, but there is a dramatic decline in both the latency and duration of the response. Comparison of our results with recent data from cortical (area 17) simple cells reveals that the temporal development of LGN cells accounts for a substantial portion of the temporal maturation of simple cells.

INTRODUCTION

Classically described as simply a relay station, the lateral geniculate nucleus (LGN) is an important processing stage within the central visual pathways. The LGN is currently thought to play a major role in regulating the flow of information from the retina to the primary visual cortex (for a review, see Casagrande and Norton 1991). Although the LGN provides the primary afferent input to striate cortex,

the receptive field (RF) organization of cortical neurons in the cat (including those in the input layers) differs dramatically from that of their LGN inputs (e.g., Hubel and Wiesel 1962). To understand the transformations that take place at the geniculate-cortical synapse, it is necessary to have a detailed understanding of the RF structure of both LGN neurons and cortical neurons.

In recent years, “white noise” techniques have been employed to map the RFs of visually responsive neurons (e.g., DeAngelis et al. 1993a; Emerson et al. 1987; Jacobson et al. 1993; Jones and Palmer 1987; McLean et al. 1994; Shapley and Reid 1991). A major advantage of these techniques is that they provide a characterization of RFs in the joint domain of space and time, and this representation yields a more comprehensive understanding of response properties than traditional static RF profiles. Thus far, nearly all of the work undertaken using these techniques has concentrated on elucidating the RF dynamics of cortical cells (see DeAngelis et al. 1995 for a review). For example, it has been shown that the RFs of simple cells can be either space-time separable or inseparable (DeAngelis et al. 1993a; McLean and Palmer 1989; McLean et al. 1994). For the latter type, the positions of RF subregions change smoothly during the time course of the response; thus, there is no unique spatial or temporal RF profile. Moreover, it has been shown that space-time inseparability constitutes a quasilinear mechanism for direction selectivity in simple cells (DeAngelis et al. 1993b; Jagadeesh et al. 1993; McLean and Palmer 1989; McLean et al. 1994; Reid et al. 1987).

How are the RFs of cortical neurons constructed from their geniculate inputs? This question remains an important topic of active research. Hubel and Wiesel (1962) initially proposed that the RF of a simple cell is constructed from a group of geniculate cells having RFs appropriately arrayed in space, a hypothesis that has recently received some direct experimental support (Chapman et al. 1991; Ferster et al. 1996; Reid and Alonso 1995). The recent characterization of simple cell RFs in the joint space-time domain has raised new questions concerning the genesis of these RFs. For example, how might LGN afferents be combined to construct the space-time inseparable RFs of direction-selective simple cells? One possibility (Saul and Humphrey 1992) is that direction-selective simple cells receive inputs from two physiologically distinct groups of LGN cells, the lagged and nonlagged cells, that have markedly different temporal response properties (Humphrey and Weller 1988; Mastrorarde 1987; Saul and Humphrey 1990). Alternatively, there could be classes of LGN cells that exhibit a form of space-time inseparability similar to simple cells. Another possibility is

that space-time inseparable RFs are constructed within the cortex, by combining the outputs of simple cells with separable RFs that differ in spatial and temporal phase (e.g., Adelson and Bergen 1985; Watson and Ahumada 1985).

To address these issues, it is essential to have a thorough, quantitative understanding of the spatiotemporal organization of LGN RFs. However, relatively little has been reported on this topic. Stevens and Gerstein (1976) performed an extensive study of the organization of LGN RFs; however, their response-plane technique did not have sufficient temporal resolution to reveal the intrinsic dynamics of the RFs. Methods utilized more recently (Eckhorn et al. 1993; Golomb et al. 1994; Reid and Shapley 1992) have overcome this problem, but data from only a few cells were presented in these reports. Hence, a major goal of the present study is to provide a detailed characterization of LGN RFs in the space-time domain.

The second major goal of this study is to examine the postnatal development of spatiotemporal RF organization in the LGN. Although previous studies have documented the developmental maturation of spatial RF properties (Daniels et al. 1978; Ikeda and Tremain 1978; Tootle and Friedlander 1989), relatively little is known about development of temporal response properties in the LGN (Daniels et al. 1978; Mangel et al. 1983). In a recent study of the postnatal development of cortical RFs in the cat (DeAngelis et al. 1993a), we found that the temporal structure of simple cell RFs matures much more slowly than the spatial structure. Thus it is of interest to determine if this difference may be accounted for at the level of the LGN.

In the study reported here, we have used a one-dimensional version of the reverse correlation technique (DeAngelis et al. 1993a; Jones and Palmer 1987) to map the spatiotemporal RFs of LGN cells recorded from adult cats and from kittens at 4 and 8 wk postnatal. Our results from adult cats reveal interesting properties of the LGN RF that can only be demonstrated in the joint space-time domain. The spatiotemporal RF profiles of most LGN cells are shown to be spatiotemporally inseparable, although the pattern of space-time inseparability shown by LGN cells is markedly different from that observed for cortical simple cells (DeAngelis et al. 1993a; McLean and Palmer 1989; McLean et al. 1994). Temporal response profiles of both the center and surround are typically biphasic, but the response of the surround is usually delayed with respect to that of the center. Moreover, the first temporal phase of the surround typically merges into the second temporal phase of the center. We show that this behavior is consistent with a simple spatiotemporal model of the LGN receptive field, in which both the center and surround profiles are space-time separable but temporally offset. RFs of lagged and nonlagged cells can be distinguished by the phase of their temporal responses, and we demonstrate that this difference can account for the characteristic response patterns of lagged cells, namely their long latency and "anomalous" offset discharge (Humphrey and Weller 1988; Mastrorarde 1987).

With regard to postnatal maturation, our results demonstrate a clear difference between the developmental time courses of spatial and temporal RF properties. The development of temporal response properties continues well beyond 8 wk postnatal. In contrast, there is very little change in the

spatial structure of LGN RFs after 4 wk postnatal. These results suggest that the prolonged maturation of temporal response properties previously observed for simple cells in the striate cortex (DeAngelis et al. 1993a) is partially accounted for by the development of subcortical structures.

METHODS

All experiments were performed with adult cats or kittens at ages 4 and 8 wk postnatal. All of the animals were reared in a normal environment. Kittens at 4 and 8 wk postnatal weighed 320–400 g and 750–1,000 g, respectively. Adult cats ranged in weight from 2.2–4.2 kg. The methods and procedures used in this study are quite similar to those we used to study spatiotemporal RF properties in the visual cortex (see DeAngelis et al. 1993a). An abbreviated version of these methods is given here with emphasis on aspects that are specific to the LGN.

Experimental preparation

Under general anesthesia, the animal is connected to equipment for life support and for continuous monitoring of vital signs (EEG, ECG, CO₂ level and intratracheal pressure). Standard surgical procedures (see DeAngelis et al. 1993a) are used to prepare the cat for single-unit recording. The animal is then secured in a stereotaxic apparatus and paralyzed with an injection of gallamine triethiodide (Flaxedil, 2%), which is subsequently infused at a rate of 10 mg · kg⁻¹ · h⁻¹ to maintain paralysis. Following the induction of paralysis, the animal is artificially respired with a gas mixture of 70% N₂O, 29% O₂, and 1% CO₂. Sodium thiamylal (Surital) is also infused at 1 mg · kg⁻¹ · hr⁻¹ to maintain adequate anesthesia. A round section of skull and dura (~5 mm in diam) is removed to allow insertion of tungsten-in-glass electrodes (Levick 1972), which have an impedance of 2–10 MΩ. For adult cats, the craniotomy is centered at Horsley-Clarke coordinates A6L9. For 4-wk-old kittens, the position of the craniotomy is set at coordinates A3L8, based on the data of Norman (1974). For 8-wk-old kittens, the craniotomy is centered halfway between the coordinates used for adult cats and 4-wk-old kittens. For kittens, we often had to adjust the position of our electrodes within the craniotomy, in order to enter the LGN near the representation of the area centralis. This is due to variation between animals in the position of the LGN within the head (Norman 1974). Pupils are dilated with atropine (1%) and nictitating membranes are retracted with 5% phenylephrine hydrochloride (Neo-Synephrine). Contact lenses (+2.0 diop.) with 3 mm artificial pupils are then positioned on each cornea.

At the end of an experiment, the animal is killed with an overdose of pentobarbital sodium (Nembutal). After perfusion and fixation with a buffered 0.9% saline solution followed by 10% formaldehyde (Formalin), the LGN is frozen and sectioned into 40 micron slices. Tissue is stained with thionin, electrode penetrations are reconstructed, and laminae are identified. Cells were recorded from all layers (A, A1, and C) of LGN, but only cells from layers A and A1 are included in this report. Cells from layer C are excluded to avoid W cells located in that layer (Cleland et al. 1976; Wilson et al. 1976). Histological analysis and the characteristic sequence of eye dominance of the cells in each penetration confirmed that all cells included in this report were recorded from layers A and A1 of LGN.

Prior to recording, the optic disks are projected, with the use of a reversible ophthalmoscope, onto a large tangent screen facing the animal. The positions of the areae centrales are then estimated from the positions of the optic disks (Milleret et al. 1988; Olson and Freeman 1978). Upon lowering the electrodes into the LGN and isolating action potentials of single neurones, the RFs are initially explored with a bar of light that is moved manually.

Recording procedures

After isolating spikes from an LGN neuron, a three stage experimental protocol is followed. 1) A preliminary search is conducted to localize the cell's RF and to determine its preferred spatial frequency (SF). 2) Quantitative measurements are obtained, with the use of drifting sinusoidal gratings, to assess the cell's selectivity for orientation, spatial frequency, and temporal frequency, as well as to classify the cell as X or Y, lagged or nonlagged. 3) A detailed spatiotemporal RF profile is obtained using the reverse correlation technique (described below). For each neuron, this three-step experimental protocol requires approximately 1.5–2.5 h to complete.

In the preliminary search procedure, the orientation, spatial frequency, position and size of a patch of drifting sinusoidal grating are controlled manually. By adjusting the parameters of the stimulus and observing the response, we obtain estimates of the cell's preferred spatial frequency and its orientation bias. By adjusting the location and size of a small patch of grating to give the largest response, the center position of the RF can be located quite accurately and the size of the RF can also be estimated.

Following this search procedure, quantitative measurements of each cell's orientation, spatial frequency, and temporal frequency tuning are obtained by presenting sequences of drifting sinusoidal gratings. Since LGN cells are excitable through only one eye (Hubel and Wiesel 1961), the stimuli are presented monocularly while the unresponsive eye views a blank CRT screen of the same mean luminance as the gratings (the CRT screens have a mean luminance of 45 cd/m², subtense of 28 × 22°, resolution of 1,024 × 804 pixels, and are refreshed at 76 Hz). The stimulus is typically a round patch of drifting, sinusoidal-luminance grating with a diameter of 10–15° and a Michelson contrast of 50%. When spatial frequency or orientation is varied, the temporal frequency of the stimulus is fixed at 2.0 Hz. To measure spatial frequency tuning, a sequence of gratings having eight different spatial frequencies (0.14–1.5 c/deg) is presented in randomized order. Each grating is presented for 4 s, during which a peristimulus time histogram (PSTH) of the response is accumulated. Successive stimuli are separated by a period of 2 s during which the animal views blank screens of the same mean luminance as the gratings. After each different stimulus is presented once, the stimulus sequence is re-randomized and presented again, until each stimulus has been shown 4–6 times. To measure the orientation bias of LGN cells (Daniels et al. 1977; Vidyasagar and Urbas 1982), a sequence of gratings is presented that spans 360° of orientation (in 12 equally spaced steps). For the temporal frequency test, spatial frequency and orientation are set to the optimal values obtained previously. Typically, eight temporal frequencies are tested in the range from 0.26–38.0 Hz. To construct tuning curves, Fourier analysis is performed on the PSTHs. The mean firing rate and the first harmonic of the response are computed.

To classify cells into X and Y types (Enroth-Cugell and Robson 1966), counterphase-modulated sinusoidal gratings are presented at several positions across the RF. For this test, the spatial frequency is adjusted to be ~1.5 octaves above the optimal value, because this provides a more sensitive probe for the Y-type nonlinearity (Hochstein and Shapley 1976). The spatial phase of the grating is varied from 0 to 180° (in 15° steps) in blocks of randomly interleaved trials. At the spatial phase that elicits the smallest response, the ratio of the second harmonic to the first harmonic is calculated (after spontaneous firing rate is subtracted). Based on the criteria of Hochstein and Shapley (1976), cells are classified as X type if the ratio is less than or equal to 1.0, whereas cells with a ratio larger than 1.0 are classified as Y type. To classify cells as lagged or nonlagged, a high contrast (90%) flashing spot is presented within the center of the RF. The luminance of the spot is modulated over time by a 1 Hz square wave (see Fig. 7, inset), and cells are classified as either lagged or nonlagged based on

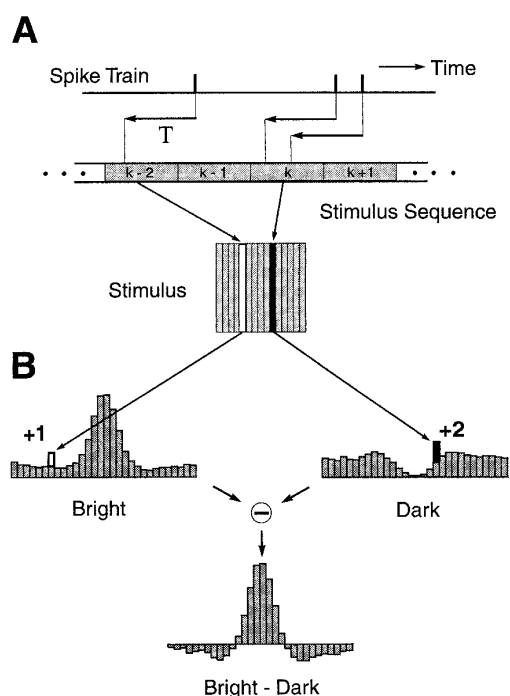


FIG. 1. To obtain detailed spatiotemporal receptive field (RF) profiles, a one-dimensional (1-D) reverse correlation algorithm is used. A: randomized sequences of long bright and dark bars (typically 15° length, 0.4–0.7° in width, and flashed for 13 or 26 ms) are presented in an area that is centered over the lateral geniculate nucleus (LGN) cell's RF. Orientation of the bars is adjusted to the optimal orientation of the cell, as estimated from stimulation with drifting sinusoidal gratings. Centers of the bars are positioned at discrete spatial locations (usually 20 or 30) along a line segment that transects the RF at an angle orthogonal to the optimal orientation (for clarity, only 15 bar positions are shown here). Assuming a correlation delay of T ms, for each spike in the recorded spike train, the position and polarity (bright or dark) of the causal stimulus is found and a histogram bin at that position is incremented. B: two histograms are initially constructed, one for responses to bright bars and one for responses to dark bars. Bins that are incremented are indicated in the graph. Bar heights in the two bins are drawn disproportionately for illustration purposes. A composite RF profile is then obtained by subtracting the dark bar responses from the bright bar responses. Composite RF profile shown here was obtained from an adult cat using a correlation delay of $T = 30$ ms. In this profile, positive values indicate excitation by a bright bar, negative values denote excitation by a dark bar.

the half-rise time of the response (Mastrorade 1987). Additional response features of lagged cells, such as the "anomalous" peak at stimulus offset, are also used in the classification (Hartveit and Heggelund 1992; Humphrey and Weller 1988; Mastrorade 1987; Saul and Humphrey 1990).

Reverse correlation analysis

To characterize the spatiotemporal RF organization of LGN cells, we used a one-dimensional (1-D) version of the reverse correlation algorithm (Jones and Palmer 1987; Palmer et al. 1991; see DeAngelis et al. 1993a for additional details). The algorithm is diagrammed schematically in Fig. 1A. The visual stimulus is a pseudo-random sequence of bright and dark bars that are presented at 20 or 30 locations across the stimulus patch shown in Fig. 1A. This stimulus patch is positioned so that its center corresponds to that of the RF, as determined in the search procedure described previously. The width of the stimulus patch is adjusted so that it covers the entire width of the RF. Since many LGN neurons are known to have an orientation bias (Daniels et al. 1977; Vidyasagar

and Urbas 1982), the orientation of the bars is adjusted to the preferred orientation of the cell, as determined from the orientation tuning curve obtained with gratings. The bar stimuli are typically 15 in length and 0.2–0.5 in width, and are usually presented for a duration of 13 ms (one video frame) or 26 ms. These parameters are varied somewhat from cell to cell, according to the spatial and temporal resolution of the RF (see DeAngelis et al. 1993a for details about choosing the spatial and temporal parameters of the reverse correlation stimulus). In general, the stimuli are chosen to be as narrow as possible in both space and time so that they still elicit a measurable response from the neuron. For cells that respond to high spatial frequencies, narrow stimuli must be used so that the spatial resolution of the reverse correlation technique is higher than that of the cell's RF, which can be determined from the spatial frequency tuning curve obtained using gratings. Similar considerations apply to the choice of stimulus duration, which can be guided by the measured temporal frequency tuning. Attention was paid to keeping the stimuli as brief as possible (13 ms for most cells from adults and 26 ms for most cells from kittens), so that temporal response profiles (e.g., Figs. 2 and 6) are not artificially extended in time (temporal blurring).

During stimulation of the RF, bars are presented one at a time in rapid succession. For each presentation, both the location of the bar in the stimulus patch and the polarity of the bar (bright or dark) are chosen randomly. A record of the stimulus sequence is stored by the computer, along with the spike train produced by an LGN cell. For a stimulus patch having 20 locations, one stimulus sequence consists of 40 different bar stimuli (20 locations \times 2 contrast polarities, dark and bright). Each different bar stimulus occurs only once during each stimulus sequence. Typically, the stimulus sequence is repeated 100–200 times in order to obtain enough spikes (on the order of several thousand) for a smooth RF profile. The time required for a complete measurement of the RF profile is in the range of 5–15 min (including a period of roughly 1.5–2 s between randomized sequences). Note that the presentation order is re-randomized each time the stimulus sequence is repeated, so that a particular temporal sequence of bright and dark bars is never repeated. During analysis of the data, each spike is assigned to the stimulus that preceded it by a delay period of T ms. In the depiction of Fig. 1A, three spikes are assigned to their likely causal stimuli, denoted by positions $k-2$, k , and k in the stimulus sequence. Because stimulus $k-2$ was a bright bar, we increment (by adding +1) a bin in the "Bright" histogram at the coordinate which corresponds to the position of the bright bar (see Fig. 1B). The stimulus k was a dark bar; thus, in the "Dark" histogram, the bin corresponding to the stimulus location is incremented twice (+2) because two spikes have been assigned to this stimulus. This assignment process is repeated for each action potential that is elicited by the stimulus sequence. In this way, separate histograms are built up over time from the responses to bright and dark bars.

Figure 1B shows a typical RF profile for an LGN cell, as obtained by our 1-D reverse correlation technique. The left and right panels show, as histograms, the response profiles for bright and dark bar stimuli, respectively. A composite RF profile is obtained by taking the difference of the bright and dark bar responses, as shown in the center panel of Fig. 1B. The assumptions underlying this subtraction operation are addressed elsewhere (see DeAngelis et al. 1993a). In the composite profile, regions excited by bright stimuli are shown as positive histogram bins, whereas regions excited by dark stimuli are shown as negative histogram bins. This composite profile describes the one-dimensional spatial structure of the RF for one particular value of the reverse correlation delay ($T = 30$ ms).

The major focus of this study is to describe the spatiotemporal dynamics of RF structure for LGN cells from cats and kittens. For this purpose, the reverse correlation algorithm is extended to

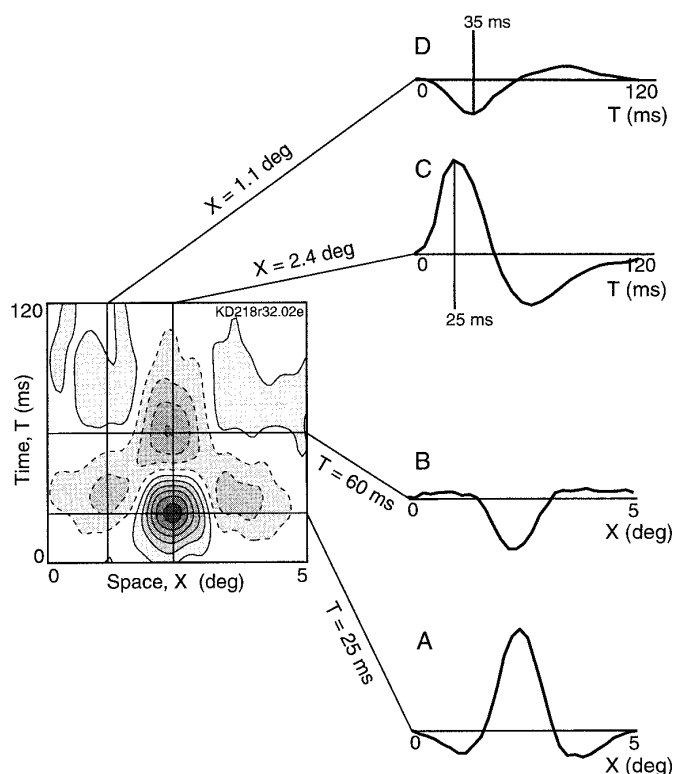


FIG. 2. Construction and interpretation of a spatiotemporal RF profile (X - T plot). *Panels A and B*: spatial RF profiles determined at two different values ($T = 25$ ms and $T = 60$ ms) of the reverse correlation delay. By obtaining additional spatial RF profiles over a range of finely spaced values of T , we derive a comprehensive picture of how spatial RF structure evolves over the time course of the response. The resulting picture is shown as a contour plot in this figure. In the contour plot, areas enclosed by solid contours correspond to bright excitatory regions, areas enclosed by dashed contours correspond to dark excitatory regions. Tick marks along the horizontal and vertical axes are drawn at 1° and 50 ms intervals, respectively. *Panels C and D*: temporal response curves obtained by slicing through the X - T data at different spatial positions (indicated by the vertical lines through the X - T plot). The curve in *panel C* is derived by slicing through the center of the RF, whereas the curve in *D* is obtained by slicing through one flank of the surround. Values shown along side the temporal response curves indicate the time delays at which the curves have their first peak (25 ms for *C*) or trough (35 ms for *D*). Stimulation parameters for this X-cell were as follows: flash duration = 13 ms, bar size = $15^\circ \times 0.5^\circ$, bar orientation = 30° , left eye.

produce a spatiotemporal RF profile (DeAngelis et al. 1993a; McLean and Palmer 1989; McLean et al. 1994). This is achieved by computing spatial RF profiles for a series of correlation delays (T) between stimulus and response. In Fig. 2, *A* and *B*, spatial RF profiles are shown for two different values of T (25 and 60 ms, respectively). By computing spatial profiles for a series of finely spaced values of T , we can construct a spatiotemporal response matrix which shows how RF structure evolves in the time domain after the onset of the stimulus. This spatiotemporal RF profile (or X - T plot), illustrated in Fig. 2, is a joint function of space (X) and time (T). Each X - T profile typically has a resolution of 20 to 30 points in both space and time. The X - T data are smoothed using a small Gaussian filter, which removes high frequency noise in the data. The parameters of this filter are chosen such that its roll-off does not substantially attenuate frequencies within the spatiotemporal pass-band of a given neuron. Once smoothed, the X - T data are interpolated and plotted as an isoamplitude contour map (see Fig. 2). Contours are drawn at 12 equally spaced amplitude levels ranging from $-A$ to $+A$, where A is the maximum absolute value

of the data. In each X - T profile, the areas enclosed by solid contour lines have positive values and represent bright-excitatory RF subregions. Areas enclosed by dashed contours have negative values and represent dark-excitatory RF subregions. The relative strengths of different subregions can be judged by the number of contour lines which enclose these regions.

Unlike previous studies in which short bars or squares were used as stimuli (Citron et al. 1981; DeAngelis et al. 1993a; Eckhorn et al. 1993; Jones and Palmer 1987), we have chosen to use long, thin bars in our reverse correlation procedure. There are several benefits of using this one dimensional mapping technique. Compared with short bars or squares, long bars often elicit a much stronger response from the neuron being tested, allowing us to obtain X - T profiles from cells that respond poorly to the full 2-D stimulus ensemble (such as many cells from young kittens). Due to increased spatial summation, these long bars are also more effective in eliciting responses from the surrounds of LGN cells. Furthermore, by restricting the stimulus to one spatial dimension, a good X - T profile can be obtained in a fraction of the time required for the 2-D method. This is very helpful when obtaining data from young kittens since recording stability is more limited in these animals. The major disadvantage associated with our 1-D algorithm is that we lose information concerning the Y dimension of the RF. Thus, for example, the elliptical RFs of many LGN cells (Cleland and Enroth-Cugell 1968), which can be seen easily in two dimensional spatial RF maps, are not revealed using our stimulus. However, our main goal is to characterize the X - T profiles of LGN cells, so this loss of information is of little consequence.

RESULTS

In this study, complete spatiotemporal receptive field profiles (X - T profiles) have been obtained for 144 LGN neurons. This population consists of 67 cells from 3 adult cats, 41 cells from 3 kittens at 8 wk postnatal, and 36 cells from 6 kittens at 4 wk postnatal. There are 56 X cells and 11 Y cells among the population from the adult cats, 34 X cells and 7 Y cells in the 8 wk population, and 32 X cells and 4 Y cells in the 4 wk population. The proportions of X and Y cells in all three age groups are similar to those reported in other studies (see Lennie 1980). Because we limited our samples to laminae A and A1, we confined our investigation to X and Y cells and avoided W cells located in the C laminae (Cleland et al. 1976; Wilson et al. 1976). Statistically, we find no significant differences between X cells and Y cells with respect to several spatial and temporal parameters of the RF (described below). However, our population of Y cells in this study is rather small. Thus, data from X and Y cells are combined in this report.

There are 4 (6.0%), 2 (4.9%), and 2 (5.6%) lagged cells in the adult, 8 wk, and 4 wk age groups, respectively, and all of the lagged cells are X-cells. These proportions of lagged cells are smaller than those reported in other studies (Hartveit et al. 1993; Mastronarde 1987; Saul and Humphrey 1990). This is likely to be due to differences in the impedance of the recording electrodes used in this and in previous studies (Mastronarde 1987; Saul and Humphrey 1990). For all cells included in this report, RFs were located within 20° of the area centralis.

General aspects of spatiotemporal RF structure

Figure 2 shows a spatiotemporal receptive field profile (X - T plot) for an ON-center LGN neuron from an adult cat

(see METHODS for details concerning the construction of X - T profiles). Spatial position (X) is plotted along the horizontal axis and time (T) is plotted on the vertical axis. As described earlier, the areas enclosed by solid contour lines have positive values and represent bright-excitatory subregions; areas enclosed by dashed contours have negative values and represent dark-excitatory subregions.

The pattern of bright- and dark-excitatory subregions seen in the X - T plot of Fig. 2 is quite typical of the vast majority of nonlagged LGN cells that we have studied (lagged cells will be discussed below; see Fig. 7). If we take a cross-section through the X - T plot at any particular value of T , the traditional center-surround organization of LGN RFs can be seen. For example, at $T = 25$ ms, the RF has a bright-excitatory center and a dark-excitatory surround (see Fig. 2A). However, at longer correlation delays, the center becomes dark-excitatory and the surround bright-excitatory (Fig. 2B).

This reversal of polarity occurs because the temporal response of the neuron is biphasic. This can be seen in Fig. 2C, which shows a temporal cross-section through the X - T data in the center of the RF. The center response of this cell has an initial bright-excitatory phase, followed by a somewhat weaker dark-excitatory phase. Although the vast majority of LGN cells have a biphasic temporal response, we have seen cells that are monophasic in time, as well as others that are triphasic. Fig. 2D shows that the temporal response of the surround is also biphasic, although substantially weaker and of opposite sign. Comparison of the temporal profiles in panels C and D of Fig. 2 reveals that the surround response is somewhat delayed relative to the response of the center. For instance, the center response reaches its first peak at a time delay of 25 ms (Fig. 2C), whereas the surround response peaks at 35 ms (Fig. 2D). This time delay between center and surround has been suggested by previous studies, based on the responses of LGN cells to gratings of varying temporal frequency (Dawis et al. 1984; Derrington and Lennie 1982; Enroth-Cugell et al. 1983; Kaplan et al. 1979). Our results provide a direct demonstration of this effect.

It should be noted here that the pattern of bright- and dark-excitatory subregions seen in the X - T plot is related to the traditional ON/OFF classification of cells (see DeAngelis et al. 1995 for details). Like the ON-center cell of Fig. 2, virtually all nonlagged cells have a temporal response profile in which the first phase is dominant (see Fig. 5E). Thus, for ON-center cells, the temporal response (of the center region) has a bright-excitatory phase followed by a dark-excitatory phase (see Fig. 2C); OFF-center cells have a dark-excitatory phase followed by one that is bright-excitatory (see Fig. 3, A and B). For lagged cells, as discussed below, these simple rules do not usually apply.

Figure 3 shows examples of X - T profiles for a representative group of LGN cells from adult cats (A and B), 8-wk-old kittens (C and D), and 4-wk-old kittens (E and F). These examples illustrate the fact that LGN RFs exhibit varying degrees of space-time inseparability. The X - T profile shown in Fig. 3D, for example, is quite separable. This means that the two-dimensional (X - T) profile, $R(X,T)$, can be well-approximated as the product of two one-dimensional

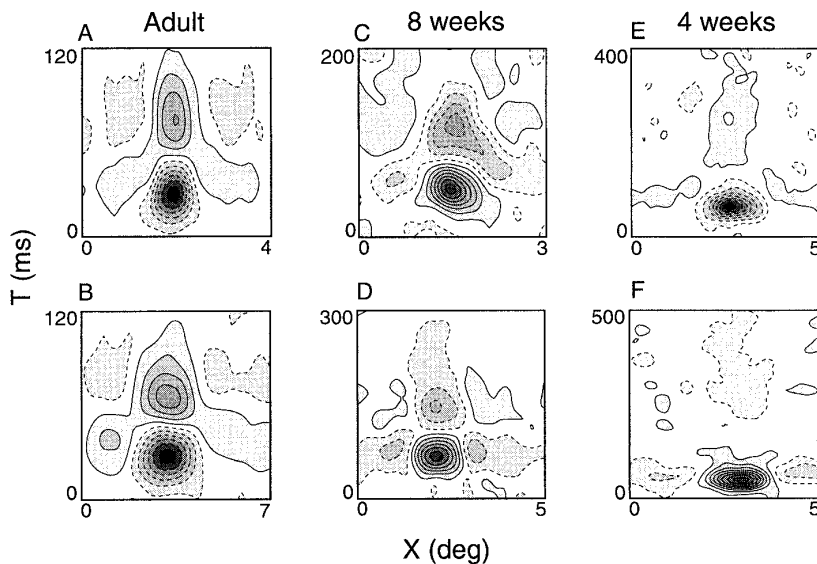


FIG. 3. X - T plots are shown for LGN cells from cats of different ages. The format of these contour plots is the same as that of Fig. 2, with horizontal and vertical tick marks corresponding to intervals of 1° and 50 ms, respectively. *A*: X - T profile for an OFF-center X-cell from an adult cat. Flash duration = 13 ms, bar size = $15^\circ \times 0.5^\circ$, bar orientation = 210° , left eye. *B*: data from another OFF-center X-cell from an adult. Flash duration = 13 ms, bar size = $20^\circ \times 0.5^\circ$, bar orientation = 200° , left eye. *C*: X - T profile for an ON-center X-cell from an 8-wk kitten. Flash duration = 26 ms, bar size = $15^\circ \times 0.3^\circ$, bar orientation = 0° , right eye. *D*: data from another ON-center X-cell from an 8-wk animal. Flash duration = 26 ms, bar size = $15^\circ \times 0.5^\circ$, bar orientation = 150° , left eye. *E*: RF profile for an OFF-center X-cell from a 4-wk kitten. Flash duration = 26 ms, bar size = $20^\circ \times 0.6^\circ$, bar orientation = 270° , left eye. *F*: data from an ON-center X-cell from a 4-wk kitten. Flash duration = 26 ms, bar size = $15^\circ \times 0.7^\circ$, bar orientation = 0° , right eye.

profiles, one a function of space, $G(X)$, and the other a function of time, $H(T)$ [i.e., $R(X,T) = G(X)*H(T)$].

In contrast, the X - T profiles shown in panels *A*, *B*, and *C* of Fig. 3 exhibit two noticeable deviations from space-time separability. As discussed for the cell of Fig. 2, the response of the surround is clearly delayed relative to that of the center. In addition, the first temporal phase of the surround response tends to blend into the second temporal phase of the center response. Thus, the two-dimensional (X - T) profile, $R(X,T)$, cannot be well approximated by the product of a function of space and a function of time (i.e., we cannot find $G(X)$ and $H(T)$ that satisfy $R(X,T) = G(X)*H(T)$). This is true for most of the LGN cells that we have studied, in all three age groups. Note, however, that the characteristic form of space-time inseparability exhibited by LGN neurons is quite different from that shown by direction-selective simple cells in visual cortex (DeAngelis et al. 1993a, 1995; McLean and Palmer 1989; McLean et al. 1994). For these simple cells, the RF subregions are oriented along an oblique axis in the space-time domain.

Inspection of the X - T profiles obtained from adult cats and kittens at 8 wk postnatal shows that they are qualitatively very similar. This is evident in Fig. 3 and applies to the vast majority of cells from these two age groups. The most noticeable difference between X - T profiles from adults and 8-wk-old kittens lies in the temporal duration of the responses (note the time scales in Fig. 3). For the adult neurons shown in panels *A* and *B* of Fig. 3, the entire spatiotemporal response profile is contained within a time epoch of 120 ms. This is typical of LGN cells from adult cats. By contrast, the X - T profiles shown in *C* and *D* fill a time epoch of 200–300 ms. Overall, the temporal profiles obtained from 8-wk kittens typically persist for much longer than those from adult cats, as shown quantitatively in the following section. For X - T profiles from the 4-wk-old kittens, the second temporal phase of the response is typically much weaker, relative to the first phase, than that seen for 8-wk kittens and adult cats. However, as seen in Fig. 3, *E* and *F*, the temporal response is quite prolonged, as compared with the profiles from older cats.

To compare the spatiotemporal RF profiles from adults and kittens, the following sections address the temporal structure and the spatial structure of the receptive fields separately. Although many LGN receptive fields are space-time inseparable, we can take temporal and spatial slices through the peak of the X - T profile, and use these slices to make quantitative comparisons between cells.

Development of temporal receptive field structure

Figure 4 illustrates the analysis we have used to quantify differences in temporal RF structure between cats of different ages. First, we find the spatial position (X) at which the X - T profile has its largest positive value (for RFs with a bright-excitatory center response) or negative value (for RFs with a dark-excitatory center response). This position is indicated by a vertical line through the X - T profile of Fig. 4*A*. A temporal response profile, $R(T)$, is then obtained by slicing through the X - T profile at this position (filled circles in Fig. 4*B*). The temporal profile is then fit with the following function:

$$F(T) = K_1 \times \frac{[c_1(T - t_{01})]^{n_1} e^{-c_1(T-t_{01})}}{n_1^n e^{-n_1}} - K_2 \times \frac{[c_2(T - t_{02})]^{n_2} e^{-c_2(T-t_{02})}}{n_2^n e^{-n_2}} \quad (1)$$

This function, $F(T)$, is the difference of two Gamma functions. K_1 , K_2 , c_1 , c_2 , t_{01} , t_{02} , n_1 , n_2 are free parameters. Our choice of this function is essentially arbitrary and is simply based on the fact that this formulation fits the data quite well (e.g., Fig. 4*B*), including the small minority of neurons that exhibit either triphasic or monophasic responses. Similar formulations have been used to model the temporal response characteristics of cortical neurons (Adelson and Bergen 1985; Watson and Ahumada 1985). A typical fit is shown as the solid curve in Fig. 4*B*. To quantitatively characterize the temporal response profile, and to facilitate comparisons between different age groups, we introduce three temporal response parameters:

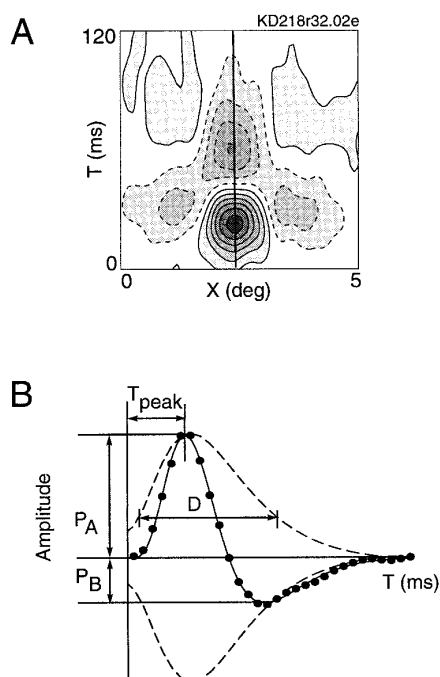


FIG. 4. Quantitative analysis of temporal response profiles. X - T data are shown for the same cell as in Fig. 2. By slicing through the peak of the X - T profile, parallel to the T axis (indicated in panel A by the vertical line), a temporal response profile (filled circles in B) is obtained. Temporal response profile is fit with the difference of two Gamma functions (see Eq. 1). Solid curve in panel B shows the best fit of Eq. 1 to the data. Three parameters are extracted from the fit. Peak response time (T_{peak}) is defined as the time at which the first peak occurs. The biphasic index is the absolute value of the ratio of the amplitude of the second peak (PB) to that of the first (PA). Duration (D) of the temporal response profile is obtained at $1/e$ (0.367) of the peak value of the temporal envelope (dashed curve).

peak response latency (T_{peak}), duration (D), and biphasic index ($\text{Rb} = |\text{PB}/\text{PA}|$) (see Fig. 4B).

The peak response latency, T_{peak} , is the value of T at which the temporal response profile has its first maximum or minimum. It indicates how fast the response of the neuron follows the onset of a stimulus. It should be noted, however, that T_{peak} is not truly an onset latency, because the cell begins to respond much earlier. Nevertheless, this parameter is convenient for comparing the time course of responses of LGN cells from adults and kittens.

By analogy to the approach used by DeAngelis et al. (1993a) for simple cells, we compute the duration (D) of the RF from the envelope of the best fitting temporal function, $F(T)$. The envelope, $E(T)$ (dashed curve in Fig. 4B), of the cell's temporal response profile is obtained as follows. First, the Hilbert transform of the temporal response function, $H[F(T)]$, is obtained by shifting the phase of all frequency components in $F(T)$ by 90 (Bracewell 1978; Gabor 1946). The temporal response function, $F(T)$, and its Hilbert transform, $H[F(T)]$, are said to form a quadrature pair. The envelope of the cell's temporal response, $E(T)$, is then computed as the vector sum of these two quadrature components

$$E(T) = \sqrt{F(T)^2 + H[F(T)]^2} \quad (2)$$

The time duration, D , of the RF is then defined as the width of the envelope, $E(T)$, at some criterion level. For conve-

nience, we have computed the duration of the temporal envelope at the level which is $1/e$ (or 0.367) of the peak envelope value. For the cell of Fig. 4, the RF duration, measured in this manner, is $D = 60$ ms.

A third useful parameter of the temporal response profile is the strength of the second phase of the response relative to the first phase. We define a biphasic index (Rb) as the ratio of the (absolute) response value at the second peak (PB) to that at the first (PA) (see Fig. 4B). The larger this index, the stronger the response of the second phase in the temporal response profile, relative to the first.

The histograms of Fig. 5 show distributions of the three temporal response parameters described above for populations of cells from adult cats and kittens. As a convention throughout this paper, black, gray, and white bars in the histograms represent data from adult cats, 8-wk postnatal kittens, and 4-wk postnatal kittens, respectively. Because some of the data shown here (and in Fig. 9) are not normally distributed, we have performed statistical analyses on the logarithm of the data. All distributions shown here are indistinguishable from normal (χ^2 , $P > 0.05$) following logarithmic transformation. The black, gray, and white arrows above the histograms show geometric means of the data for the three populations.

Figure 5A shows the distribution of T_{peak} for a population of 67 LGN cells from adult cats, 41 cells from 8-wk postnatal kittens, and 36 cells from 4-wk postnatal kittens. The geometric mean values, as indicated by the arrows, are 35.9, 58.2, and 55.4 ms for cells from adults, 8-wk kittens, and 4-wk kittens, respectively.

Figure 5B shows the mean values of T_{peak} plotted as a function of age. Error bars show the 95% confidence interval for each mean value. According to the Tukey criterion, if the 95% confidence intervals of two mean values overlap, these two values are not significantly different ($P > 0.05$). If there is no overlap of the error bars, the two mean values are significantly different ($P < 0.05$). It is clear from Fig. 5B that the peak response latency of LGN cells is about the same for kittens at 4 and 8 wk, and then declines significantly from 8 wk postnatal to adulthood (ANOVA: $F(2,141) = 48.8$, $P < 0.001$).

The histograms of Fig. 5C show the distributions of RF duration, D , for the same three populations of cells. The geometric means are 79.6, 115.9, and 108.0 ms for adults, 8-wk kittens, and 4-wk kittens, respectively. Fig. 5D shows the mean values of D plotted as a function of age. Notice again that the mean values of response duration for 8-wk and 4-wk kittens are similar, whereas the duration for adults is substantially shorter (ANOVA: $F(2,141) = 28.8$, $P < 0.001$).

Fig. 5E shows distributions of the biphasic index (Rb) for the different age groups. The geometric means are 0.41, 0.44, and 0.20 for adults, 8-wk kittens, and 4-wk kittens, respectively. Fig. 5F shows the mean values of Rb plotted as a function of age. Unlike the results for T_{peak} and D , the biphasic index is not significantly different between 8-wk kittens and adult cats, but it is significantly smaller for the 4-wk kittens (ANOVA: $F(2,141) = 29.5$, $P < 0.001$). This means that the second phase of the temporal response for 4-wk kittens is, on average, substantially weaker than its counterpart for 8-wk kittens and adult cats. Note also that

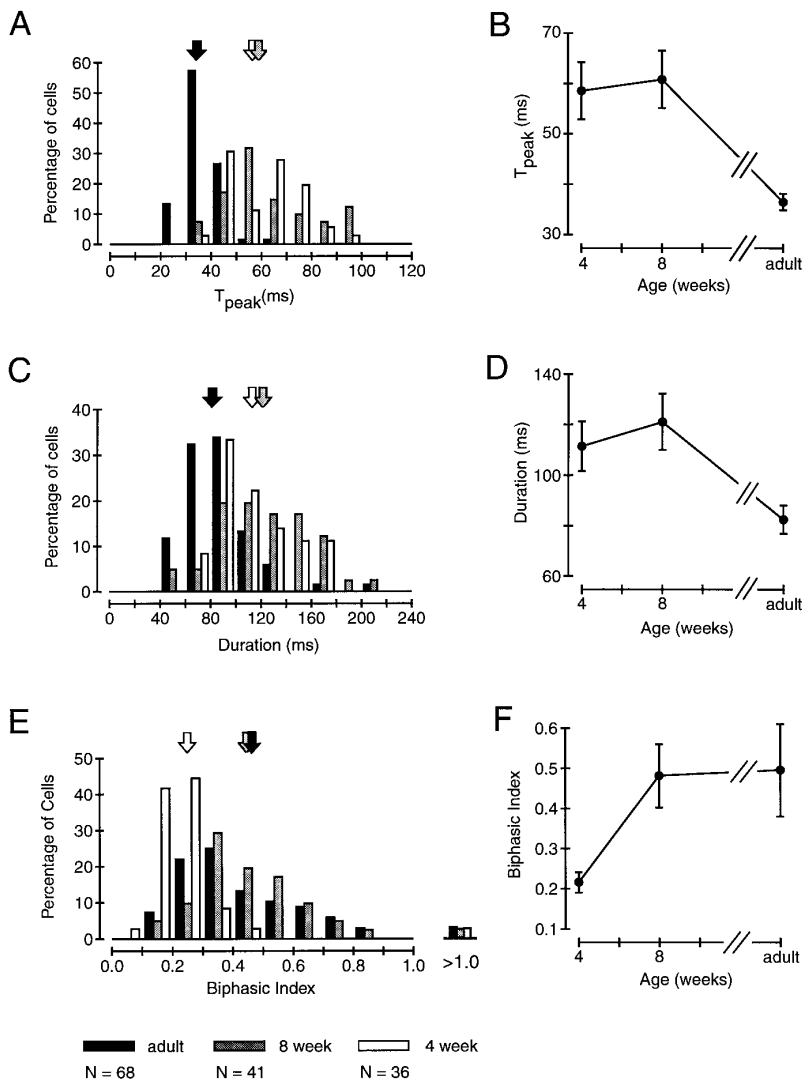


FIG. 5. Postnatal development of temporal RF parameters. *A*: histogram showing distributions of T_{peak} for the three age groups. Black, grey, and white bars denote data from adult cats, 8-wk kittens, and 4-wk kittens, respectively. Black, grey, and white arrows above the histograms indicate the geometric means for each population. *B*: mean values of T_{peak} plotted as a function of age. Error bars represent 95% confidence intervals. By the Tukey criterion, if the error bars overlap, then two values are not significantly different (at $P > 0.05$ since 95% confidence intervals are used). *C*: distributions of response D for adult cats and kittens. Conventions as in *A*. *D*: mean duration plotted as a function of age. *E*: histogram of the biphasic indices of temporal response profiles. *F*: mean biphasic indices for the different age groups.

only a few LGN cells had a biphasic index larger than 1. This occurs when the second phase of the temporal response has a larger amplitude than the first phase (e.g., Fig. 7, *A* and *C*). These neurons were all lagged cells, as discussed below.

To summarize the changes in temporal RF structure that occur during postnatal development, we have constructed a summary temporal response profile for the three populations of cells. For each neuron, we normalize the best-fitting temporal response profile [$F(T)$; Eq. 1] to have a peak value of 1.0. We then average these profiles (point by point) for all of the cells recorded in each age group. These summary profiles are plotted in Fig. 6*A*. From 4 wk to 8 wk postnatal, there is a clear increase in the strength of the second temporal response phase, with little change in the peak response latency or response duration. From 8 wk postnatal to adulthood, the shape of the temporal response profile remains similar but there is a clear temporal scaling (i.e., compression) of the response. Thus, the development of temporal RF structure seems to occur in two stages (see DISCUSSION for more on this point).

Figure 6*B* shows summary temporal response profiles separately for ON-center and OFF-center cells. To facilitate com-

parison between ON- and OFF-center responses within each age group, the average temporal profiles for OFF-center cells (dashed curves) are inverted. There is little difference between ON- and OFF-center cells with respect to the shape of the temporal response profile.

Lagged and nonlagged cells

LGN cells in the cat can be divided into lagged and nonlagged types based on the temporal response pattern exhibited in response to a flashing spot stimulus (Humphrey and Weller 1988; Mastrorarde 1987). Using a similar test (described below; see also METHODS), we also find it possible to distinguish lagged and nonlagged cells.

Given that lagged and nonlagged cells differ in their temporal properties, how are these differences reflected in the structure of the X - T profile? X - T plots for lagged and nonlagged cells are shown, respectively, in panels *A* and *B* of Fig. 7.

Although both cells give a sustained ON response to a spot of light presented within the RF center (see Fig. 7, *E* and *F*), they clearly differ in their temporal RF structures. This can be seen by comparing temporal cross-sections

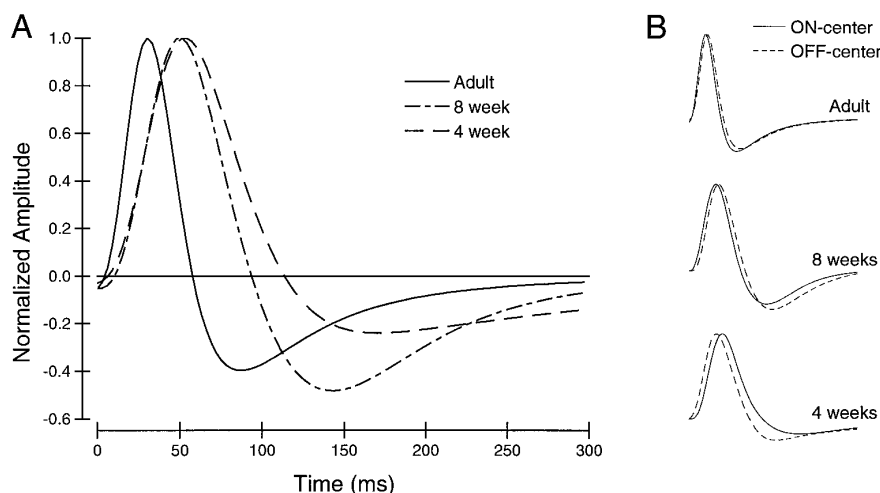


FIG. 6. Summary of developmental changes in temporal RF structure. *A*: temporal response profiles for populations of neurons (both ON- and OFF-center) from adult cats (solid curve), 8-wk kittens (dot-dashed curve), and 4-wk kittens (dashed curve). Each curve is generated by averaging the best-fitting temporal response curves for all cells within the same age group. In doing so, the sign of the responses was inverted for OFF-center cells, to avoid cancellation. Notice that from 4 wk to 8 wk, the predominant change is an increase in the strength of the second phase of the response, whereas from 8 wk to adulthood, the change is approximately a scaling in the time domain. *B*: comparison between ON and OFF center cells for each age group. Summary temporal profiles for the OFF center cells are inverted for easier comparison.

through the center of the X - T data, which are shown in Fig. 7, *C* and *D*. For the lagged cell (Fig. 7*C*), the temporal response profile has an initial dark-excitatory phase followed by a much larger bright-excitatory phase, and then a second weak dark-excitatory phase. The nonlagged cell (Fig. 7*D*) is typical in that it has a large bright-excitatory phase followed by a weaker dark-excitatory phase. Thus the difference between the temporal responses of lagged and nonlagged cells can be characterized as a temporal phase shift. Saul and Humphrey (1990) reached the same conclusion by inferring the temporal response profile from temporal frequency tuning curves. Our results show that the temporal phase shift is clearly revealed in the spatiotemporal RF profile. Given that our sample of lagged neurons is very small, however, further work will clearly be necessary to quantify differences in spatiotemporal RF structure between lagged and nonlagged cells.

To understand how a temporal phase shift in the spatiotemporal receptive field might lead to the characteristic response properties of lagged cells to a flashing spot, we have

generated a linear prediction from the X - T data and have compared this prediction with the actual response to a flashing spot. Panels *E* and *F* of Fig. 7 show, in PSTH form, the responses of our example lagged and nonlagged cells to a spot of light flashed on and off (1.0 Hz square wave) in the center of the RF. To make a direct comparison between the X - T data and the flashing spot response, it is first necessary to remove the spontaneous activity from the PSTH and to compensate for the effects of a response threshold. This is done by taking the raw response histogram to a flashing spot and subtracting off a replica that has been phase shifted by 180° (one-half cycle). The resulting PSTHs are shown in Fig. 7, *E* and *F* (thin curves). Note that these PSTHs represent an artificial construct, and that response levels below zero would normally not be observable due to a response threshold.

To obtain a linear prediction of the response to a flashing spot, we convolve the spot stimulus with the X - T data, under the assumption that the RF behaves linearly. The results of this prediction are shown as the thick curves in Fig. 7, *E*

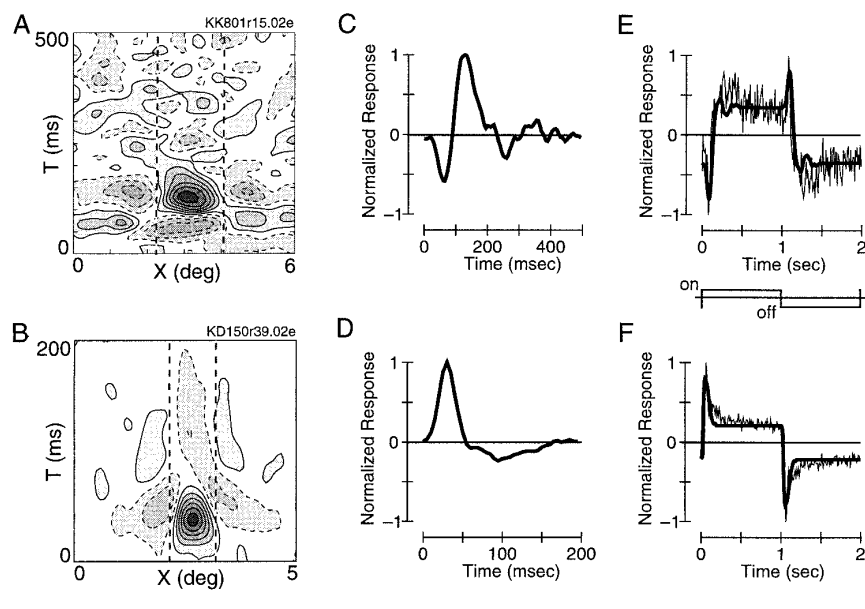


FIG. 7. This figure highlights the major differences between lagged and nonlagged cells in the temporal domain. On the left are X - T profiles for a lagged X -cell from an 8-wk kitten (*A*) and a nonlagged X -cell from an adult cat (*B*). To predict the cells' responses to a flashing spot, a portion of the X - T profile (delimited by the dashed lines), which corresponds to the size and location of the spot stimulus, is summed over space. Resulting temporal response profiles are shown in panels *C* and *D*. Notice that for the lagged cell, the amplitude of the second peak of the response is larger; whereas for the nonlagged cell, the first response peak dominates. Temporal response profiles in *C* and *D* are then convolved with the temporal waveform of the flashing spot stimulus (between panels *E* and *F*) to obtain linear predictions of the cells' flash responses. These predicted responses (thick curves) are shown in panels *E* and *F*, along with the measured responses (thin curves) to the flashing spot stimulus. The PSTHs shown in *E* and *F* are normalized and span one temporal cycle of the stimulus. Stimulation parameters for the X - T data in *A*: flash duration = 26 ms, bar size = $15^\circ \times 0.7^\circ$, bar orientation = 90° , right eye. For the X - T data in *B*: flash duration = 13 ms, bar size = $15^\circ \times 0.4^\circ$, bar orientation = 90° , left eye.

and F . Clearly, the major features in the response pattern of the lagged and nonlagged cells are captured by the linear prediction. For the lagged ON-center cell (Fig. 7E), the (observable) response to stimulus onset is delayed by ~ 130 ms because of a brief but powerful suppression at the beginning of the response. This suppression is a direct consequence of the fact that the cell's temporal response (Fig. 7C) has an initial dark-excitatory phase preceding the dominant bright-excitatory phase. An anomalous offset discharge, which is characteristic of lagged cells, can also be seen in the linear prediction of Fig. 7E. For the nonlagged ON-center cell (Fig. 7F), there is a transient, short-latency onset response, followed by a sustained plateau.

These results show that the distinguishing response properties of lagged cells can be predicted reasonably well, assuming linear summation, from the temporal structure of the RF profile.

Development of spatial receptive field structure

In this section, we examine how spatial aspects of LGN RFs mature during normal postnatal development. The spatial properties that we consider are RF center size, surround size, and the relative strengths of the center and surround responses.

To analyze spatial structure, we extract a spatial RF profile from the X - T data, and compare it between the different age groups. A 1-D spatial profile is obtained by slicing horizontally through the X - T data at $T = T_{\text{peak}}$ (indicated by the horizontal line through the X - T plot in Fig. 8A). Filled circles in Fig. 8B show the raw spatial profile, obtained in this manner, for a typical ON-center X-cell.

The 1-D spatial profile exhibits the classical center-surround RF organization. This structure has often been modeled as a difference of Gaussians (DOG) function (Rodieck 1965). It has also been reported that the RF profiles of LGN cells may be asymmetric (e.g., Dawis et al. 1984). This can be seen in Fig. 8B, where the strengths of the two flanks of the surround are slightly dissimilar. Some degree of asymmetry is exhibited by many of the cells that we have studied. This behavior can be accounted for by a model in which the RF is described in terms of a difference of two Gaussian components that may be spatially offset (Dawis et al. 1984; Enroth-Cugell et al. 1983).

The RFs of Y-cells have been reported to consist of a linear component, which is qualitatively similar to the RFs of X cells, and a nonlinear component, which consists of many small subunits that exhibit nonlinear spatial summation (Hochstein and Shapley 1976). We have not found any evidence that these nonlinear subunits are represented in the X - T data for Y cells. Thus we conclude that the X - T profiles that we obtain for Y cells represent only the linear response component. This issue will be addressed in considerably more detail in another paper (D. Cai, G. DeAngelis, and R. Freeman, unpublished results).

We have fit the 1-D spatial RF profiles of X and Y cells with a modified difference of Gaussians (DOG) function, given by

$$F(X) = A_c \times e^{-(X-x_c)^2/\sigma_c^2} - A_s \times e^{-(X-x_s)^2/\sigma_s^2} \quad (3)$$

In this formulation, A_c and A_s are the amplitudes of the

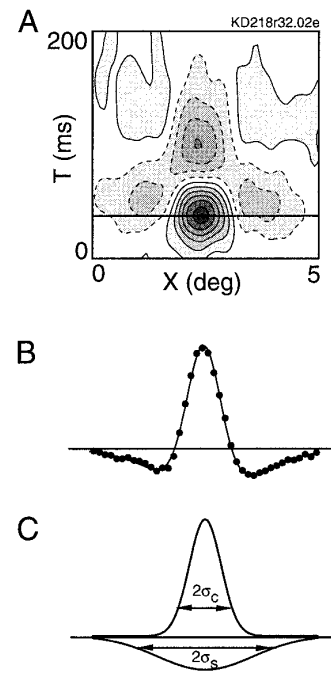


FIG. 8. The fitting procedure used to quantify spatial aspects of LGN RF structure is illustrated here. *A*: an X - T profile is shown for an ON-center X-cell recorded from an adult cat (same cell as in Figs. 2 and 4). *B*: a 1-D spatial RF profile (filled circles) is obtained by taking a cross section through the X - T data at $T = T_{\text{peak}}$, as indicated by the horizontal line through the X - T plot in Fig. 8A). Solid curve represents a difference of Gaussians (DOG) function that best fits the spatial profile. *C*: center and surround components of the best-fitting DOG function are shown here. Parameters $2\sigma_c$ and $2\sigma_s$ (see Eq. 3) are used as metrics of the sizes of the RF center and surround, respectively.

center and surround Gaussians, $2\sigma_c$ and $2\sigma_s$ are the respective sizes of the center and surround (defined as the full width of the Gaussian at a criterion level of 0.367 times the amplitude), and x_c , x_s give the center positions of the two components. The solid curve in Fig. 8B shows the DOG function that best fits the spatial RF profile of this adult LGN X-cell. Figure 8C shows the two Gaussian components of the fit. Parameters of the best-fitting DOG function have been used to compare the RFs of LGN cells recorded from adult cats and kittens.

The histograms in Fig. 9 show distributions of three spatial parameters: center size ($2\sigma_c$; Fig. 9A), surround size ($2\sigma_s$; Fig. 9C), and surround/center amplitude ratio (A_s/A_c ; Fig. 9E). Data from adult cats, 8-wk kittens and 4-wk kittens are represented in black, gray, and white, respectively. Because most of the data in Fig. 9 are not normally distributed, statistical analyses were performed on the logarithm of the data. All distributions were indistinguishable from normal (χ^2 , $P > 0.05$) after logarithmic transformation. Figure 9A shows distributions of RF center size ($2\sigma_c$) for the three age groups. The geometric means are 1.22° , 1.37° , and 1.15° for adult cats, 8-wk kittens, and 4-wk kittens, respectively. Figure 9B plots the (geometric) mean values of RF center size as a function of age. There is no significant trend for center size to change with age (ANOVA, $F(2,141) = 1.53$, $P = 0.22$). The mean values of RF center size for the different age groups are not significantly different (Tukey criterion, $P > 0.05$).

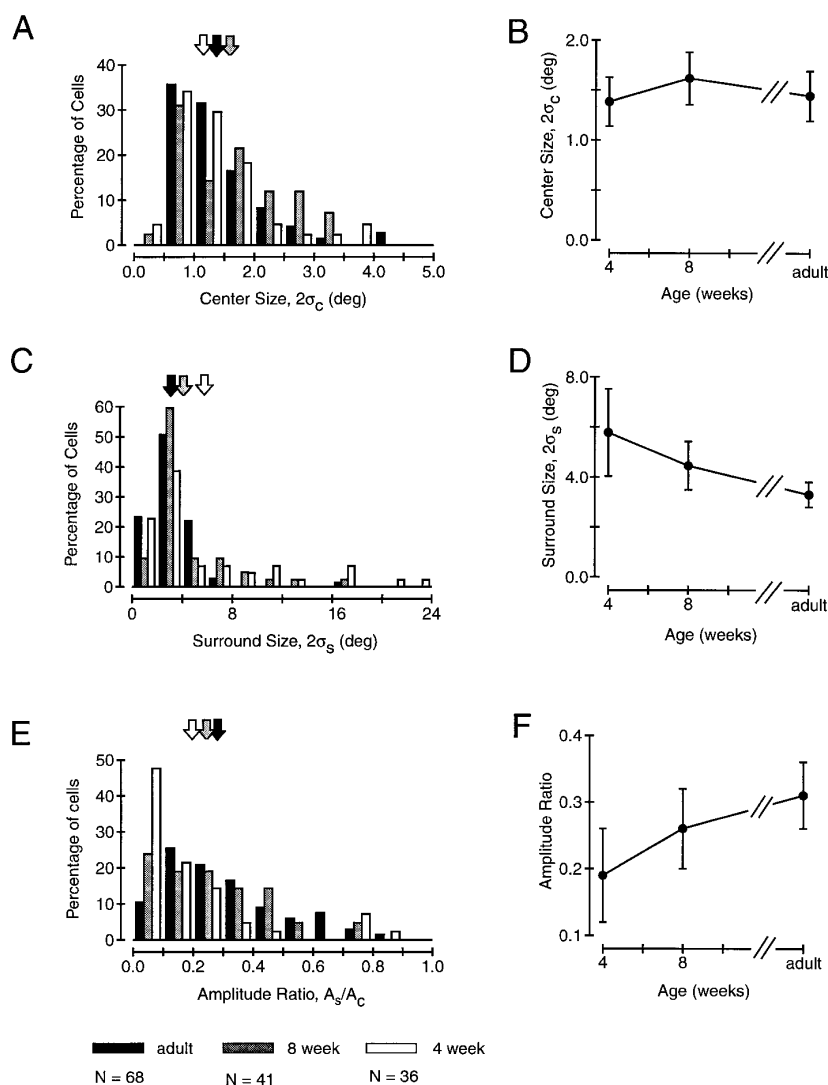


Figure 9C shows distributions of the size of the surround ($2\sigma_s$) for the three age groups. The geometric means of surround size are 2.95° , 3.69° , and 3.98° for adult cats, 8-wk kittens, and 4-wk kittens, respectively. One-way ANOVA reveals a weakly significant trend for the surround size to decrease with age [$F(2,141) = 3.14$, $P = 0.046$], but the mean values of surround size for the three age groups are not significantly different (Tukey, $P > 0.05$).

Another important aspect of spatial RF organization is the relative strength of the center and surround components. We introduce an amplitude ratio parameter (A_s/A_c) in which A_s is surround amplitude and A_c is center amplitude, to quantify the relative strengths of the center and surround. The stronger the surround response, the larger the value of this ratio. Figure 9E shows the distributions of the A_s/A_c ratios for adult cats and kittens. The geometric means are 0.25, 0.20, and 0.10 for adult cats, 8-wk kittens, and 4-wk kittens, respectively. Figure 9F shows how the amplitude ratio changes with age. ANOVA shows that there is a significant trend for the amplitude ratio to increase with age [$F(2,141) = 17.5$, $P < 0.001$]. The amplitude ratios for adult cats and 8-wk kittens are not significantly different.

However, the mean amplitude ratio of the 4-wk kittens is significantly smaller than that of the other two age groups (Tukey, $P < 0.05$).

In the same way that we constructed summary temporal response profiles for each age group (see Fig. 6), we construct summary spatial response profiles by averaging together the best-fitting spatial RF profiles [$F(X)$; Eq. 3] of all cells in each age group. Fig. 10A shows population curves obtained by combining data from ON-center and OFF-center cells. Before averaging, the profiles for OFF-center cells are inverted so that the center response is always positive; in addition, the spatial profiles of all cells are shifted so that the central peaks are aligned. If there is a spatial offset between the center and surround, the surround is always shifted to one side of the center (i.e., toward positive position values in Fig. 10A) to prevent the asymmetries in the spatial profiles of different cells from canceling each other.

Fig. 10A shows that there are only modest changes in the spatial structure of LGN RFs after 4 wk postnatal, whereas Fig. 6 shows that there are dramatic changes in the temporal structure of these RFs. Fig. 10B shows separate summary profiles for ON-center and OFF-center cells. In general, there

FIG. 9. Quantitative summary of changes in spatial RF parameters with age. The format of this figure is identical to that of Fig. 5. *A*: histogram of RF center size ($2\sigma_c$) for cats of different ages. *B*: RF center size plotted against age. Filled circles give the geometric mean and error bars represent the 95% confidence interval. *C*: distributions of the surround size, $2\sigma_s$, are shown in this histogram. *D*: changes in mean surround size ($2\sigma_s$) for cats of different ages. *E*: histogram showing the ratio of the amplitudes (A_s/A_c) of the surround and center components of the RF for LGN cells from cats of different ages. *F*: the mean surround/center amplitude ratio (A_s/A_c) is plotted against age.

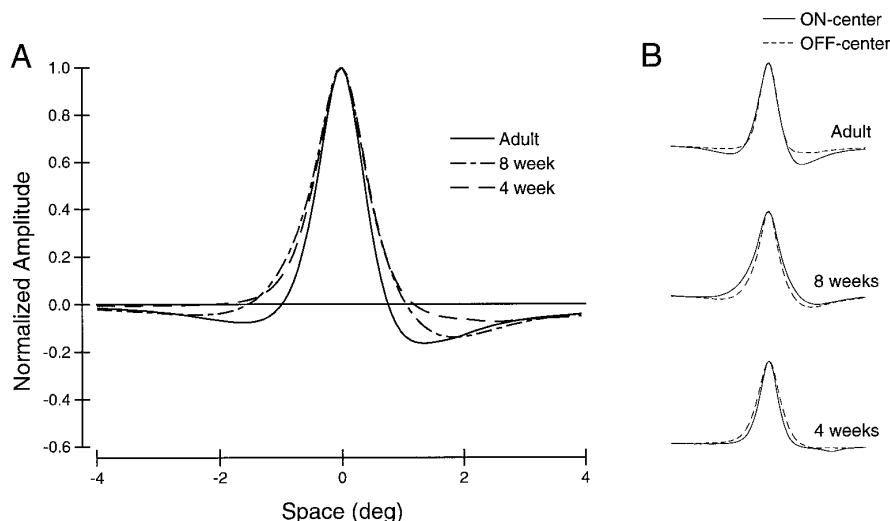


FIG. 10. Population summary of developmental changes in spatial RF structure. The format of this figure is identical to that of Fig. 6. *A*: summary spatial RF profiles are shown for populations of cells (including both ON- and OFF-center units) from adults and kittens. *B*: summary profiles are shown separately for ON- and OFF-center cells.

is no major difference between the spatial profiles of ON- and OFF-center cells, except that the surrounds of OFF-center cells from adult cats are somewhat weaker than those of ON-center cells. Overall, the data of Figs. 6 and 10 show that the spatial organization of LGN RFs matures earlier than the temporal structure.

A spatiotemporal RF model for LGN cells

Having characterized the spatiotemporal RFs of LGN neurons, we wish to construct a simple model that can account for the main features of the data. It is well established that a difference of Gaussians (DOG) function (Rodieck 1965) provides a good fit to the spatial sensitivity profiles of retinal ganglion and LGN cells. However, to fit our data, we need an explicit formulation for the temporal RF profile. Moreover, we need to account for varying degrees of spatiotemporal inseparability in the data. Our initial observations (e.g., Fig. 2, *C* and *D*) suggested that this might be achieved by expanding the traditional DOG model to include a variable delay between center and surround responses. Similar formulations have been proposed (Dawis et al. 1984; Enroth-Cugell et al. 1983) to explain spatiotemporal coupling in the frequency domain (see DISCUSSION).

Our model consists of two space-time separable components, one for the center and one for the surround. Each of the separable components has a Gaussian spatial profile and a temporal profile that is modeled as the difference of two Gamma functions (as described earlier; see Eq. 1). The temporal response profiles of the center and surround components are identical, except for a time delay. Thus, the complete X - T model will be space-time separable if the delay between center and surround is zero, and inseparable otherwise (see also Enroth-Cugell et al. 1983). The expressions for the model are as follows

$$R(X, T) = F_{\text{center}}(X)G_{\text{center}}(T) + F_{\text{surround}}(X)G_{\text{surround}}(T) \quad (4)$$

where

$$F_{\text{center}}(X) = A_c \times e^{-(X-x_c)^2/\sigma_c^2} \quad (5)$$

$$G_{\text{center}}(T) = K_1 \times \frac{[c_1(T - t_{01})]^{n_1} e^{-c_1(T-t_{01})}}{n_1! e^{-n_1}} - K_2 \times \frac{[c_2(T - t_{02})]^{n_2} e^{-c_2(T-t_{02})}}{n_2! e^{-n_2}} \quad (6)$$

$$F_{\text{surround}}(X) = A_s \times e^{-(X-x_s)^2/\sigma_s^2} \quad (7)$$

$$G_{\text{surround}}(T) = G_{\text{center}}(T - t_d) \quad (8)$$

Notice that the temporal function for the surround [$G_{\text{surround}}(T)$] is the same as that for the center [$G_{\text{center}}(T)$] except for the time delay (t_d).

In Fig. 11, the left column of panels *A*, *B*, and *C* shows the measured X - T profiles for three LGN cells. The cell in row *A* has a spatiotemporally separable RF, with slight spatial asymmetry. The cell in row *B* is clearly spatiotemporally inseparable, and has a small spatial asymmetry. The cell in *C* is somewhat inseparable and approximately spatially symmetric. The middle column of Fig. 11 shows the best fits of the model to the raw X - T profiles. Clearly, the fits are quite good and capture the major features of the X - T profiles. The right-most column of Fig. 11 shows the spatial and temporal component functions of the model: $F_{\text{center}}(X)$, $F_{\text{surround}}(X)$, $G_{\text{center}}(T)$, and $G_{\text{surround}}(T)$. For the spatiotemporally separable RF in row *A*, the temporal response profiles of the center and the surround have no temporal offset; thus, they are superimposed. In this case, the temporal response profiles of the center and surround are indistinguishable. For the spatiotemporally inseparable cells in *B* and *C*, the temporal response profiles of the surrounds are clearly delayed with respect to their respective center components. Similarly, the offset of the spatial components in rows *A* and *B* can explain the spatial asymmetry of the RFs.

The average values (\pm SE) of the time delay, t_d , between center and surround are 6.4 ± 0.8 ms for adult cats, 8.8 ± 1.1 ms for 8-wk kittens, and 16.3 ± 1.2 ms for 4-wk kittens. ANOVA reveals that there is a significant trend [$F(2,121) = 24.2$, $P < 0.001$] for t_d to decrease with age.

In conclusion, although more complicated models may describe the X - T data more completely, our simple model captures the most salient features of the X - T profiles. Thus,

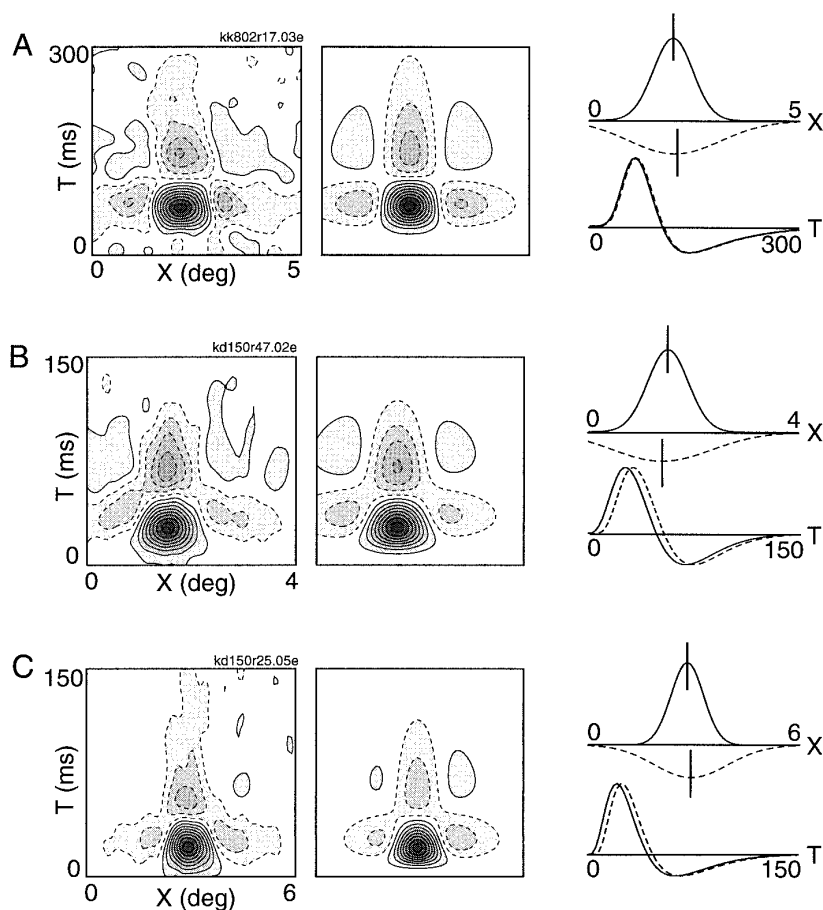


FIG. 11. This figure shows a simple model that accounts for the major features of the spatiotemporal RF profiles of LGN neurons. On the *left* are X - T profiles for three typical LGN neurons. In the *middle* are fits to the X - T data using the model of Eq. 4. On the *right* are the spatial and temporal components of the respective fits for each cell. Solid curves show the components of the center response and dashed curves are those for the surround. Vertical bars through the spatial components indicate the center position of the Gaussian functions. See text for further details.

it appears that a simple extension of the traditional DOG model is sufficient to explain the spatiotemporal dynamics of LGN RFs.

DISCUSSION

In this study, we have applied a one-dimensional version of the reverse correlation technique to examine the spatiotemporal RF organization of LGN neurons in adult cats, as well as in kittens at the ages of 4 and 8 wk postnatal. The reverse correlation technique is well-suited to reveal important basic features of the LGN RF. We have investigated the center-surround organization, spatial symmetry of the center and the surround, temporal response profiles of lagged cells and nonlagged cells, and the interactions between space and time (i.e., separability). Our spatiotemporal maps of LGN RFs consist of clear center and surround regions. As reported previously (e.g., Dawis et al. 1984), the two flanks of the surround are not of equal strength for many of the LGN RF maps. This asymmetry appears to be caused by a spatial offset of the center and surround (see below). Most of the RF maps show biphasic temporal response profiles for both the center and the surround. However, there are cells that have multiphasic temporal response profiles. Most of these cases involve lagged cells, for which the temporal response profile is phase shifted such that the second temporal phase dominates the response. Many of the LGN RF maps are spatiotemporally inseparable. The inseparability is

primarily a result of the surround response being delayed relative to that of the center. In addition, the first temporal phase of the surround often converges toward the second temporal phase of the center. This kind of space time inseparability, shown in LGN neurons, is clearly different from that exhibited by cortical simple cells (see DeAngelis et al. 1993a, 1995; McLean and Palmer 1989; McLean et al. 1994).

By comparing the spatiotemporal RFs of adult cats and kittens at different postnatal ages, we have characterized the maturation of spatiotemporal RFs during normal postnatal development. Our results demonstrate a clear difference in developmental time course between spatial and temporal properties. The development of temporal response properties continues well beyond 8 wk postnatal, whereas there is very little change in the spatial structure of LGN RFs after 4 wk postnatal. These results roughly parallel those found for simple cells in the visual cortex (DeAngelis et al. 1993a). Therefore, the prolonged maturation of temporal response properties of cortical cells may be accounted for to some extent by the development of subcortical structures.

The spatiotemporal organization of LGN receptive fields

The RFs of neurons in the retino-geniculo-cortical pathway were originally described simply as functions of space (e.g., Hubel and Wiesel 1962; Kuffler 1953). In recent years, technically advanced methods for RF mapping have allowed

a complete characterization of RFs in the joint domain of space and time (see DeAngelis et al. 1995 for a review). The majority of this work has focused on elucidating the spatiotemporal RF structure of cortical neurons (DeAngelis et al. 1993a; Eckhorn et al. 1993; Emerson et al. 1987; Jacobson et al. 1993; McLean and Palmer 1989; Shapley and Reid 1991). However, to better understand the genesis of cortical RFs, it is also important to have a clear understanding of the spatiotemporal RF structure of the main cortical inputs, namely those from the LGN. Stevens and Gerstein (1976) first examined the space-time organization of LGN RFs in an elegant study; however, their “response-plane” technique did not have sufficient temporal resolution to reveal the intrinsic temporal dynamics of single neurons. Nevertheless, a number of their conclusions are consistent with ours. More recently, researchers have used “white-noise” techniques to characterize the RF dynamics of retinal ganglion cells (Citron et al. 1981, 1988) and LGN cells (Eckhorn et al. 1993; Golomb et al. 1994; Reid and Shapley 1992). However, in these studies, data from only a few neurons were presented. To our knowledge, the present study is the first systematic, quantitative investigation of spatiotemporal RF structure for a sizeable population of LGN neurons. Related work from other laboratories has appeared in abstract form, however (Alonso et al. 1995; Reid and Shapley 1990; Wolfe et al. 1994).

An important concept to emerge from studies of cortical RFs is that of space-time inseparability. If a RF is inseparable, then it can only be described adequately in the joint space-time domain (Adelson and Bergen 1985; DeAngelis et al. 1993a; Reid et al. 1991) there is no unique spatial (or temporal) RF profile. Our data show that many LGN cells exhibit some degree of inseparability. This space-time coupling is manifested (e.g., Fig. 2) as a delay of the surround response relative to the center response and as a blending of the center and surround responses during the time-course of the response. This form of inseparability is quite different, however, from that exhibited by direction-selective simple cells (see DeAngelis et al. 1993a; McLean and Palmer 1989; McLean et al. 1994), which have RF subregions that are oriented obliquely in the X - T domain. A similar type of inseparability is not observed in the LGN. Thus, it remains to be understood exactly how the inseparable RFs of simple cells are constructed (see DeAngelis et al. 1995; Saul and Humphrey 1992 for further discussion).

The spatial organization of LGN RFs has been modeled successfully as a difference of Gaussians (DOG) function (e.g., Dawis et al. 1984). Having now extended the description of LGN RFs to the joint space-time domain, we sought to determine whether the classical DOG model can be generalized to describe the space-time data. In our modified DOG model (see Fig. 11 and related text), the center and surround components are each space-time separable, but the surround response may be delayed relative to that of the center. We have found that this simple modification provides for an excellent fit to the X - T profiles of most LGN cells.

It should be noted that our LGN RF model is essentially identical to the model used by Enroth-Cugell et al. (1983) to fit the spatiotemporal frequency spectra of retinal ganglion cells. Thus, the space-time inseparability exhibited by both ganglion and LGN cells appears to be well accounted for

by a temporal delay of the surround response. A similar, but slightly more complicated, model was proposed by Dawis et al. (1984) to fit the spatiotemporal frequency response of ganglion and LGN cells. In this model, both the center/surround amplitude ratio and the temporal phase between center and surround were allowed to vary with temporal frequency. Dawis et al. (1984) concluded that their data were consistent with a separable center mechanism and an inseparable surround mechanism. Although we have not compared these models directly, the results of our simulations suggest that the simple “temporal delay” model is sufficient to account for the basic structure observed in our RF profiles.

Development of LGN receptive field organization

Postnatal development of neuronal response properties in the cat's visual system has been the subject of numerous studies (for reviews, see Fregnac and Imbert 1984; Mitchell and Timney 1984). Because the dorsal LGN provides the predominant input to the visual cortex, the spatiotemporal development of LGN RFs is of considerable interest. Previous physiological studies of LGN development (Daniels et al. 1978; Ikeda and Tremain 1978; Mangel et al. 1983; Tootle and Friedlander 1989) have focused almost exclusively, however, on spatial RF organization. In this study, we have directly compared the development of temporal and spatial properties for the same populations of neurons.

Our data show that the developmental maturation of temporal RF structure continues well past the age of 8 wk postnatal. Specifically, both the peak response latency (T_{peak}) and response duration (D) decline markedly from 8 wk postnatal to adulthood. These results are consistent with previous findings that the latency of LGN responses to optic chiasm stimulation declines gradually from 4 wk postnatal to adulthood (Daniels et al. 1978; Mangel et al. 1983). Interestingly, our population results (Fig. 6) suggest that temporal RF structure matures in two distinct stages. From 4 wk to 8 wk, there is a marked change in the shape of the temporal RF profile, with a substantial strengthening of the second response phase (Fig. 6A). However, there is little, if any, change in the response latency or duration during this time period. From 8 wk postnatal to adulthood, the shape of the response profile remains approximately the same, but there is a notable shortening of the time-scale of the response (i.e., temporal compression). This two-stage pattern of temporal development suggests that there may be different mechanisms at work during these two periods, although measurements at more finely spaced time intervals are required to fully address the “two-stage” hypothesis.

In contrast to the large changes in temporal RF structure that we have observed after 4 wk postnatal, we find relatively little change in the spatial structure of LGN RFs from 4 wk of age to adulthood (Fig. 10A). Our finding that spatial structure is almost mature at 4 wk is consistent with a preponderance of previous evidence from studies of developing retinal ganglion cells (Hamasaki and Flynn 1977; Rusoff and Dubin 1977) and LGN cells (Daniels et al. 1978; Norman et al. 1977; Tootle and Friedlander 1989), particularly as regards X-cells. Consistent with previous studies, we do observe a modest decline (Fig. 9D) in the size of RF surrounds

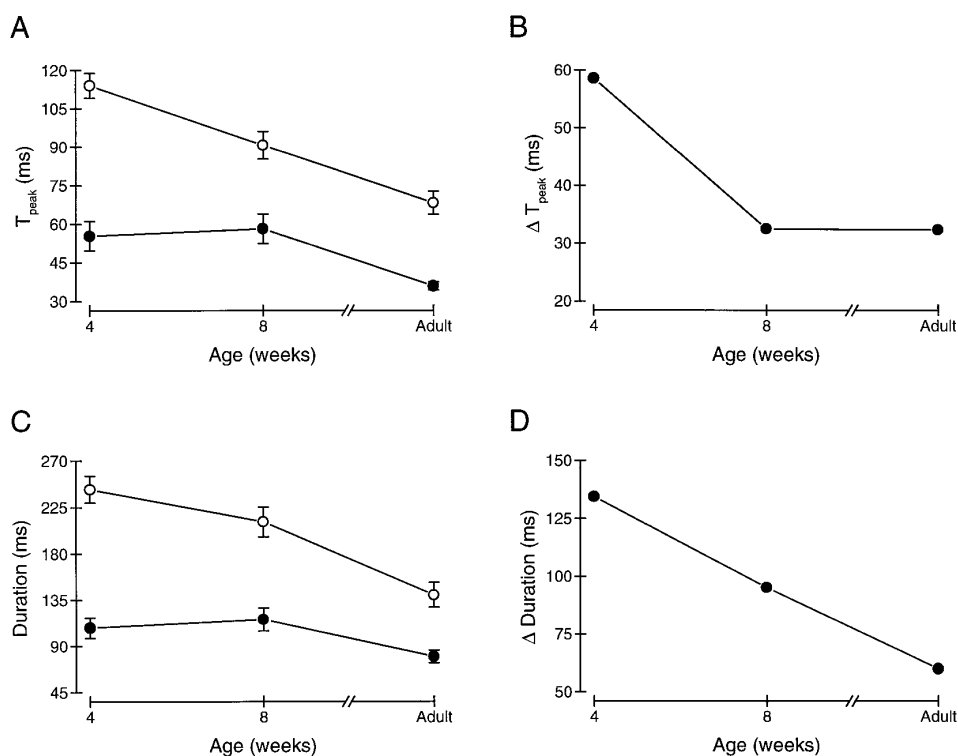


FIG. 12. Comparison of postnatal development of temporal response properties for LGN cells and cortical simple cells. *A*: change in peak response latency (T_{peak}) as a function of age for populations of LGN cells (filled circles; replotted from Fig. 5*B*) and simple cells [open circles; replotted from Fig. 5*C* of DeAngelis et al. (1993a)]. *B*: difference between mean values of T_{peak} for simple cells and LGN cells is plotted as a function of age. *C*: developmental change in RF duration for populations of LGN cells (filled circles; replotted from Fig. 7*B*) and simple cells [open circles; replotted from Fig. 7*B* of DeAngelis et al. (1993a)]. *D*: difference in mean duration between simple and LGN RFs as a function of age.

(Rusoff and Dubin 1977; Tootle and Friedlander 1989), as well as a concomitant increase (Fig. 9*F*) in the strength of surround inhibition (Daniels et al. 1978). We do not find any significant decrease in RF center sizes (Fig. 9*B*) after 4 wk postnatal. This is in agreement with some previous reports on X-cells (Rusoff and Dubin 1977 for ganglion cells; Daniels et al. 1978); however, other studies report a modest decline in RF center size after 4 wk postnatal (Ikeda and Tremain 1978; Tootle and Friedlander 1989). Since these differences are small, they may be attributable to sampling biases, to differences in the range of eccentricities studied, or to the degree of accuracy attained in measuring RF size.

In summary, comparison of Fig. 6*A* with Fig. 10*A* shows that changes in temporal RF structure occur much later during development than changes in spatial RF structure. This finding may account to some degree for the similar recent observations made regarding cortical simple cells (DeAngelis et al. 1993a), as discussed below.

Comparison with cortical simple cells

We reported previously (DeAngelis et al. 1993a) that the temporal RF structure of cortical cells continues to mature well past the age of 8 wk postnatal. A summary of these findings is plotted in Fig. 12, *A* and *C*, along with the comparable data for LGN neurons from the present study. Panels *B* and *D* of Fig. 12 show the mean differences between pools of simple cells and LGN cells, with respect to peak latency (T_{peak}) and RF duration (*D*), as a function of age.

The data of Fig. 12 highlight several interesting points. First, the mean values of T_{peak} and duration for LGN cells are substantially smaller than those for simple cells, and this fact holds for each age group. The responses of simple cells

peak later and are substantially more prolonged than those of LGN cells. Thus, simple cells have substantially poorer temporal resolution than LGN cells at all ages, a result which agrees with previous findings from adults [compare Baker (1990) and DeAngelis et al. (1993b) with Troy (1983); see also Hawken et al. (1996)]. The mechanisms underlying this loss of temporal resolution at the geniculo-cortical synapse are not entirely clear, but convergence of multiple geniculate inputs (of varying latencies) onto a simple cell may account for at least part of the effect.

The data of Fig. 12 are also quite revealing in terms of mechanisms of temporal development. If the temporal development of a simple cell's RF were determined entirely by that of its geniculate inputs, then we would expect the difference curves in Fig. 12, *B* and *D* to be flat. On the other hand, if the temporal development of simple cells was determined solely by changes in intracortical circuitry, then one would expect the LGN curves in Fig. 12, *A* and *C* to be flat, while the simple cell curves declined. Clearly, the data lie somewhere between these two extreme possibilities. Although temporal selectivity improves with age in both areas, there does appear to be an early component of development that is mainly intracortical. Both T_{peak} and duration decline substantially for simple cells between 4 wk and 8 wk postnatal, whereas the corresponding values for LGN neurons remain essentially unchanged during this time period.

With regard to spatial RF structure, our findings suggest that there is, again, a cortical component of development. Previous work has shown that the size of RF subregions of simple cells decreases between 4 wk and 8 wk postnatal (Braastad and Heggelund 1985; DeAngelis et al. 1993a). On the other hand, our present results show that RF center size in the LGN remains approximately constant from 4 wk postnatal to adulthood. This finding suggests that the LGN

inputs to simple cells become more accurately aligned in space during postnatal maturation, an interpretation that is consistent with reports that geniculate-cortical axonal arbors go through extensive pruning after birth (e.g., Shatz 1990).

We are grateful to A. Anzai for help in conducting these experiments and to Izumi Ohzawa for development of reverse correlation software, as well as assistance with data analysis.

This work was supported by research and CORE grants from the National Eye Institute (EY-01175 and EY-03176) and by a collaborative project of the Human Frontiers Science Program.

Present address of G. C. DeAngelis: Dept. of Neurobiology, Stanford University School of Medicine, Stanford, CA 94305-5401.

Address for reprint requests: R. D. Freeman, University of California, 360 Minor Hall, Berkeley, CA 94720-2020.

REFERENCES

- ADELSON, E. H. AND BERGEN, J. R. Spatiotemporal energy models for the perception of motion. *J. Opt. Soc. Am.* 2: 284-299, 1985.
- ALONSO, J. M., ATTICK, J. J., AND REID, R. C. The temporal responses of LGN receptive fields studied with white noise (Abstract). *Invest. Ophthalmol. Visual Sci. Suppl.* 36: 689, 1995.
- BAKER, C., JR. Spatial- and temporal-frequency selectivity as a basis for velocity preference in cat striate cortex neurons. *Visual Neurosci.* 4: 101-113, 1990.
- BRAASTAD, B. O. AND HEGGELUND, P. Development of spatial receptive-field organization and orientation selectivity in kitten striate cortex. *J. Neurophysiol.* 53: 1158-1178, 1985.
- BRACEWELL, R. N. *The Fourier Transform and Its Applications*. New York: McGraw-Hill, 1978.
- CASAGRANDE, V. A. AND NORTON, T. T. Lateral geniculate nucleus: a review of its physiology and function. In: *Vision and Visual Dysfunction. The Neural Basis of Visual Function*, edited by A. G. Leventhal. Boca Raton, FL: CRC Press, 1991, p. 41-84.
- CHAPMAN, B., ZAHS, K. R., AND STRYKER, M. P. Relation of cortical cell orientation selectivity to alignment of receptive fields of the geniculocortical afferents that arborize within a single orientation column in ferret visual cortex. *J. Neurosci.* 11: 1347-1358, 1991.
- CITRON, M. C., EMERSON, R. C., AND LEVICK, W. R. Nonlinear measurement and classification of receptive fields in cat retinal ganglion cells. *Ann. Biomed. Eng.* 16: 65-77, 1988.
- CITRON, M. C., KROEKER, J. P., AND MCCANN, G. D. Nonlinear interactions in ganglion cell receptive fields. *J. Neurophysiol.* 46: 1161-1176, 1981.
- CLELAND, B. G. AND ENROTH-CUGELL, C. Quantitative aspects of sensitivity and summation in the cat retina. *J. Physiol. (Lond.)* 198: 17-38, 1968.
- CLELAND, B. G., LEVICK, W. R., MORSTYN, R., AND WAGNER, H. G. Lateral geniculate relay of slowly conducting retinal afferents to cat visual cortex. *J. Physiol. (Lond.)* 255: 299-320, 1976.
- DANIELS, J. D., NORMAN, J. L., AND PETTIGREW, J. D. Biases for oriented moving bars in lateral geniculate nucleus neurons of normal and stripe-reared cats. *Exp. Brain Res.* 29: 155-172, 1977.
- DANIELS, J. D., PETTIGREW, J. D., AND NORMAN, J. L. Development of single-neuron responses in kitten's lateral geniculate nucleus. *J. Neurophysiol.* 41: 1373-1393, 1978.
- DAWIS, S., SHAPLEY, R., KAPLAN, E., AND TRANCHINA, D. The receptive field organization of X-cells in the cat: spatiotemporal coupling and asymmetry. *Vision Res.* 24: 549-564, 1984.
- DEANGELIS, G. C., OHZAWA, I., AND FREEMAN, R. D. Spatiotemporal organization of simple-cell receptive fields in the cat's striate cortex. I. General characteristics and postnatal development. *J. Neurophysiol.* 69: 1091-1117, 1993a.
- DEANGELIS, G. C., OHZAWA, I., AND FREEMAN, R. D. Spatiotemporal organization of simple-cell receptive fields in the cat's striate cortex. II. Linearity of temporal and spatial summation. *J. Neurophysiol.* 69: 1118-1135, 1993b.
- DEANGELIS, G. C., OHZAWA, I., AND FREEMAN, R. D. Receptive-field dynamics in the central visual pathways. *Trends Neurosci.* 18: 451-458, 1995.
- DERRINGTON, A. M. AND LENNIE, P. The influence of temporal frequency and adaptation level on receptive field organization of retinal ganglion cells in cat. *J. Physiol. (Lond.)* 333: 343-366, 1982.
- ECKHORN, R., KRAUSE, F., AND NELSON, J. I. The RF-cinematogram. A cross-correlation technique for mapping several visual receptive fields at once. *Biol. Cybern.* 69: 37-55, 1993.
- EMERSON, R. C., CITRON, M. C., VAUGHN, W. J., AND KLEIN, S. A. Nonlinear directionally selective subunits in complex cells of cat striate cortex. *J. Neurophysiol.* 58: 33-65, 1987.
- ENROTH-CUGELL, C. AND ROBSON, J. G. The contrast sensitivity of retinal ganglion cells of the cat. *J. Physiol. (Lond.)* 187: 517-552, 1966.
- ENROTH-CUGELL, C., ROBSON, J. G., SCHWEITZER-TONG, D. E., AND WATSON, A. B. Spatio-temporal interactions in cat retinal ganglion cells showing linear spatial summation. *J. Physiol. (Lond.)* 341: 279-307, 1983.
- FERSTER, D., CHUNG, S., AND WHEAT, H. Orientation selectivity of thalamic input to simple cells of cat visual cortex. *Nature* 380: 249-252, 1996.
- FREGNAC, Y. AND IMBERT, M. Development of neuronal selectivity in primary visual cortex of cat. *Physiol. Rev.* 64: 325-434, 1984.
- GABOR, D. Theory of communication. *J. Inst. Electr. Engrg.* 93: 429-457, 1946.
- GOLOMB, D., KLEINFELD, D., REID, R. C., SHAPLEY, R. M., AND SHRAIMAN, B. I. On temporal codes and the spatiotemporal response of neurons in the lateral geniculate nucleus. *J. Neurophysiol.* 72: 2990-3003, 1994.
- HAMASAKI, D. I. AND FLYNN, J. T. Physiological properties of retinal ganglion cells of 3-week-old kittens. *Vision Res.* 17: 275-284, 1977.
- HARTVEIT, E. AND HEGGELUND, P. The effect of contrast on the visual response of lagged and nonlagged cells in the cat lateral geniculate nucleus. *Visual Neurosci.* 9: 515-525, 1992.
- HARTVEIT, E., RAMBERG, S. I., AND HEGGELUND, P. Brain stem modulation of spatial receptive field properties of single cells in the dorsal lateral geniculate nucleus of the cat. *J. Neurophysiol.* 70: 1644-1655, 1993.
- HAWKEN, M. J., SHAPLEY, R. M., AND GROSF, D. H. Temporal-frequency selectivity in monkey visual cortex. *Visual Neurosci.* 13: 477-492, 1996.
- HOCHSTEIN, S. AND SHAPLEY, R. M. Quantitative analysis of retinal ganglion cell classifications. *J. Physiol. (Lond.)* 262: 237-264, 1976.
- HUBEL, D. H. AND WIESEL, T. N. Integrative action in the cat's lateral geniculate body. *J. Physiol. (Lond.)* 155: 385-398, 1961.
- HUBEL, D. H. AND WIESEL, T. N. Receptive fields, binocular interaction, and functional architecture in the cat's visual cortex. *J. Physiol. (Lond.)* 160: 106-154, 1962.
- HUMPHREY, A. L. AND WELLER, R. E. Functionally distinct groups of X-cells in the lateral geniculate nucleus of the cat. *J. Comp. Neurol.* 268: 429-447, 1988.
- IKEDA, H. AND TREMAIN, K. E. The development of spatial resolving power of lateral geniculate neurones in kittens. *Exp. Brain Res.* 31: 193-206, 1978.
- JACOBSON, L. D., GASKA, J. P., CHEN, H. W., AND POLLEN, D. A. Structural testing of multi-input linear-nonlinear cascade models for cells in macaque striate cortex. *Vision Res.* 33: 609-626, 1993.
- JAGADEESH, B., WHEAT, H. S., AND FERSTER, D. Linearity of summation of synaptic potentials underlying direction selectivity in simple cells of the cat visual cortex. *Science* 262: 1901-1904, 1993.
- JONES, J. P. AND PALMER, L. A. The two-dimensional spatial structure of simple receptive fields in cat striate cortex. *J. Neurophysiol.* 58: 1187-1211, 1987.
- KAPLAN, E., MARCUS, S., AND SO, Y. T. Effects of dark adaptation on spatial and temporal properties of receptive fields in cat lateral geniculate nucleus. *J. Physiol. (Lond.)* 294: 561-580, 1979.
- KUFFLER, S. W. Discharge patterns and functional organization of mammalian retina. *J. Neurophysiol.* 16: 37-68, 1953.
- LENNIE, P. Parallel visual pathways: a review. *Vision Res.* 20: 561-594, 1980.
- LEVICK, W. R. Another tungsten microelectrode. *Med. Biol. Eng.* 10: 510-515, 1972.
- MANGEL, S. C., WILSON, J. R., AND SHERMAN, S. M. Development of neuronal response properties in the cat dorsal lateral geniculate nucleus during monocular deprivation. *J. Neurophysiol.* 50: 240-264, 1983.
- MASTRONARDE, D. N. Two classes of single-input X-cells in cat lateral geniculate nucleus. I. Receptive-field properties and classification of cells. *J. Neurophysiol.* 57: 357-380, 1987.
- MCLEAN, J. AND PALMER, L. A. Contribution of linear spatiotemporal receptive field structure to velocity selectivity of simple cells in area 17 of cat. *Vision Res.* 29: 675-679, 1989.
- MCLEAN, J., RAAB, S., AND PALMER, L. A. Contribution of linear mechanisms to the specification of local motion by simple cells in areas 17 and 18 of the cat. *Visual Neurosci.* 11: 271-294, 1994.
- MILLERET, C., BUISSERET, P., AND GARY-BOBO, E. Area centralis position

- relative to the optic disc projection in kittens as a function of age. *Invest. Ophthalmol. Visual Sci.* 29: 1299–1305, 1988.
- MITCHELL, D. E. AND TIMNEY, B. Postnatal development of function in the mammalian visual system. In: *Handbook of Physiology. The Nervous System. Sensory Processes*. Washington, DC: Am. Physiol. Soc., 1984, p. 507–555.
- NORMAN, J. L. *Development of Field Responses of the Lateral Geniculate Nucleus in Kittens* (Ph.D. dissertation). Riverside, CA: University of California, 1974.
- NORMAN, J. L., PETTIGREW, J. D., AND DANIELS, J. D. Early development of X-cells in kitten lateral geniculate nucleus. *Science* 198: 202–204, 1977.
- OLSON, C. R. AND FREEMAN, R. D. Eye alignment in kittens. *J. Neurophysiol.* 41: 848–859, 1978.
- PALMER, L. A., JONES, J. P., AND STEPNIOSKI, R. A. Striate receptive fields as linear filters: characterization in two dimensions of space. In: *Vision and Visual Dysfunction. The Neural Basis of Visual Function*, edited by A. G. Leventhal. Boca Raton, FL: CRC Press, 1991, p. 246–265.
- REID, R. C. AND ALONSO, J. M. Specificity of monosynaptic connections from thalamus to visual cortex. *Nature* 378: 281–284, 1995.
- REID, R. C. AND SHAPLEY, R. M. Spatial and temporal characteristics of cone inputs to macaque LGN cells as mapped by pseudorandom stimuli (Abstract). *Invest. Ophthalmol. Visual Sci. Suppl.* 31: 429, 1990.
- REID, R. C. AND SHAPLEY, R. M. Spatial structure of cone inputs to receptive fields in primate lateral geniculate nucleus. *Nature* 356: 716–718, 1992.
- REID, R. C., SOODAK, R. E., AND SHAPLEY, R. M. Linear mechanisms of directional selectivity in simple cells of cat striate cortex. *Proc. Natl. Acad. Sci. USA* 84: 8740–8744, 1987.
- REID, R. C., SOODAK, R. E., AND SHAPLEY, R. M. Directional selectivity and spatiotemporal structure of receptive fields of simple cells in cat striate cortex. *J. Neurophysiol.* 66: 505–529, 1991.
- RODIECK, R. W. Quantitative analysis of cat retinal ganglion cell response to visual stimuli. *Vision Res.* 5: 583–601, 1965.
- RUSOFF, A. C. AND DUBIN, M. W. Development of receptive-field properties of retinal ganglion cells in kittens. *J. Neurophysiol.* 40: 1188–1198, 1977.
- SAUL, A. B. AND HUMPHREY, A. L. Spatial and temporal response properties of lagged and nonlagged cells in cat lateral geniculate nucleus. *J. Neurophysiol.* 64: 206–224, 1990.
- SAUL, A. B. AND HUMPHREY, A. L. Evidence of input from lagged cells in the lateral geniculate nucleus to simple cells in cortical area 17 of the cat. *J. Neurophysiol.* 68: 1190–1208, 1992.
- SHAPLEY, R. M. AND REID, R. C. Spatiotemporal receptive fields and direction selectivity. In: *Computational Models of Visual Processing*, edited by M. S. Landy and J. A. Movshon. Cambridge, MA: MIT Press, 1991, p. 109–118.
- SHATZ, C. J. Impulse activity and the patterning of connections during CNS development. *Neuron* 5: 745–756, 1990.
- STEVENS, J. K. AND GERSTEIN, G. L. Spatiotemporal organization of cat lateral geniculate receptive fields. *J. Neurophysiol.* 39: 213–238, 1976.
- TOOTLE, J. S. AND FRIEDLANDER, M. J. Postnatal development of the spatial contrast sensitivity of X- and Y-cells in the kitten retinogeniculate pathway. *J. Neurosci.* 9: 1325–1340, 1989.
- TROY, J. B. Spatio-temporal interaction in neurones of the cat's dorsal lateral geniculate nucleus. *J. Physiol. (Lond.)* 344: 419–432, 1983.
- VIDYASAGAR, T. R. AND URBAS, J. V. Orientation sensitivity of cat LGN neurones with and without inputs from visual cortical areas 17 and 18. *Exp. Brain Res.* 46: 157–169, 1982.
- WATSON, A. B. AND AHUMADA, A., JR. Model of human visual-motion sensing. *J. Opt. Soc. Am.* 2: 322–341, 1985.
- WILSON, P. D., ROWE, M. H., AND STONE, J. Properties of relay cells in cat's lateral geniculate nucleus: a comparison of W-cells with X- and Y-cells. *J. Neurophysiol.* 39: 1193–1209, 1976.
- WOLFE, J. N., WOLLMAN, D. E., AND PALMER, L. A. Spatiotemporal receptive field structure of lagged cells in the cat LGN (Abstract). *Invest. Ophthalmol. Visual Sci. Suppl.* 35: 1662, 1994.